Bioorganic & Medicinal Chemistry 17 (2009) 7964–7970

Contents lists available at ScienceDirect

Bioorganic & Medicinal Chemistry

journal homepage: www.elsevier.com/locate/bmc

Bioorganic synthesis of a recombinant HIV-1 fusion inhibitor, SC35EK, with an N-terminal pyroglutamate capping group

Kazumi Kajiwara [a,b], Kentaro Watanabe [a], Rei Tokiwa [a,b], Tomoko Kurose [a,b], Hiroaki Ohno [a], Hiroko Tsutsumi [c], Yoji Hata [c], Kazuki Izumi [d], Eiichi Kodama [d], Masao Matsuoka [d], Shinya Oishi [a,*], Nobutaka Fujii [a,*]

[a] Graduate School of Pharmaceutical Sciences, Kyoto University, Sakyo-ku, Kyoto 606-8501, Japan
[b] JST Innovation Plaza Kyoto, Japan Science and Technology Agency, Nishigyo-ku, Kyoto 615-8245, Japan
[c] Gekkeikan Research Institute, Gekkeikan Sake Company, Ltd, Fushimi-ku, Kyoto 612-8391, Japan
[d] Institute for Virus Research, Kyoto University, Sakyo-ku, Kyoto 606-8507, Japan

ARTICLE INFO

Article history:
Received 10 September 2009
Revised 7 October 2009
Accepted 8 October 2009
Available online 13 October 2009

Keywords:
Anti-HIV peptide
Fusion inhibitor
HIV
Pyroglutamate

ABSTRACT

The bioorganic synthesis of an end-capped anti-HIV peptide from a recombinant protein was investigated. Cyanogen bromide-mediated cleavage of two Met-Gln sites across the target anti-HIV sequence generated an HIV-1 fusion inhibitor (SC35EK) analog bearing an N-terminal pyroglutamate (pGlu) residue and a C-terminal homoserine lactone (Hsl) residue. The end-capped peptide, pGlu-SC35EK-Hsl, had similar bioactivity and biophysical properties to the parent peptide, and an improved resistance to peptidase-mediated degradation was observed compared with the non-end-capped peptide obtained using standard recombinant technology.

1. Introduction

Human immunodeficiency virus type 1 (HIV-1) is an enveloped virus that causes acquired immunodeficiency syndrome (AIDS) through the infection of immune cells. A number of anti-HIV drugs that target key enzymes in HIV-1 life cycle, including reverse transcriptase and viral protease, have been employed for highly active anti-retroviral therapy (HAART). Although combination therapy by HAART achieves prolonged viral suppression, resistant variants against these drugs often appear and compromise therapeutic efficiency.[1] In order to manage this disease, novel anti-HIV drugs that target existing classes of molecules as well as newly identified molecules in the viral replication cycle have been developed, such as entry inhibitors and HIV-1 integrase inhibitors.[2]

The fusion inhibitors are a new class of therapeutics for the treatment of HIV-1-infected patients. These drugs prevent viral entry into cells,[3] which is mediated by the conformational transition of the viral envelope protein gp41[4] that occurs after gp120 binds to its receptors on the host cell surface. The ectodomain of gp41, with two heptad repeat regions, HR1 and HR2, is folded into an anti-parallel coiled-coil structure of fusion-active conformation. Synthetic peptides derived from gp41 HR2, such as T-20 (enfuvirtide) and C34, exert potent anti-HIV activity by interfering with this viral gp41 folding and, therefore, the subsequent membrane fusion process.[5,6] The mode of interaction between an inhibitory HR2 peptide and the viral HR1, including a representative peptide N36, has been elucidated and exploited to design the second-generation of fusion inhibitors.[7] Previously, we developed the potent anti-HIV peptides, T-20EK and SC35EK, which were designed by rearrangement of the bioactive α-helix structure of T-20 and C34, respectively.[8] Substitutions of the non-interactive residues within T-20 and C34 with hydrophilic glutamic acids or lysines improved the anti-HIV activity of the original peptides as well as their biophysical properties.

T-20 is manufactured by chemical synthesis, in which a combination of solid-phase and solution-phase peptide synthesis methods is employed.[9] Chemical synthesis of peptides allows optional modifications at the appropriate residues or positions by using non-proteinogenic amino acids and/or special amino acids with post-translational modifications which prolonged the effects of the peptide therapeutics in vivo. For example, N-terminal acyl- and/or C-terminal amide-modified peptides can be easily prepared, which can then contribute to the protection from enzymatic scissions that may occur in the circulatory system. However, step-wise elongation of a peptide-chain using protected amino acid components may be disadvantageous in terms of cost-effectiveness and environmental acceptability. The expression of recombinant

* Corresponding authors. Tel.: +81 75 753 4551; fax: +81 75 753 4570.
E-mail addresses: soishi@pharm.kyoto-u.ac.jp (S. Oishi), nfujii@pharm.kyoto-u.ac.jp (N. Fujii).

0968-0896/$ - see front matter © 2009 Elsevier Ltd. All rights reserved.
doi:10.1016/j.bmc.2009.10.017

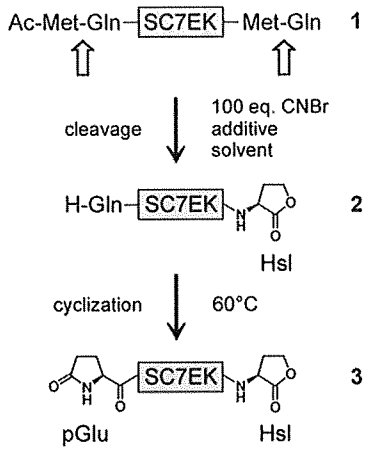

Scheme 1.

proteins is an alternative approach used to prepare bioactive peptides and proteins,[10] but the products are normally obtained without any functional modifications. Taking advantage of this approach, we synthesized an anti-HIV peptide, SC35EK, by a combination of the recombinant expression of fusion proteins in *Escherichia coli* and their subsequent treatment with chemical reagents to incorporate end-capping groups at both the N- and C-termini.

Among the several cleavage reactions available for peptides and proteins, cyanogen bromide (CNBr)-mediated cleavage at methionine (Met) residues is one of the most conventional, and is used for both sequence analysis and for the preparation of bioactive, short peptides from insoluble recombinant fusion proteins in *E. coli*. Such proteins include antibiotic peptides,[11] zinc finger peptides,[12] insulin-like peptides[13] and pH-responsive self-assembling peptides.[14] It is noteworthy that CNBr-mediated cleavage releases the first fragment containing a cyclic homoserine lactone (Hsl) at the C-terminus,[15] and the second fragment without any N-terminal functional group. This Hsl residue was designed as a C-terminal protecting group for SC35EK. Pyroglutamic acid (pGlu) was chosen as the N-terminal protecting group as this residue is important for the physiological stability of several mammalian peptide hormones and proteins.[16] The cyclic structure of pGlu can be obtained by cyclization from a glutamine (Gln) residue mediated either by glutaminyl cyclase in vivo, or by treatment of Gln in non-enzymatic conditions.[16,17]

In this study, we undertook the bioorganic synthesis of an SC35EK analog, which contains cyclic N-terminal pGlu and C-terminal Hsl end-capping structures.[18] Using a model synthetic peptide, the conditions necessary for the cleavage and cyclization of a Gln residue to a pGlu residue were optimized. Recombinant His-tag fusion proteins containing either a single, or three consecutive anti-HIV sequences were expressed and purified from *E. coli*. The peptide, pGlu-SC35EK-Hsl, was cleaved from the resulting recombinant protein under optimized acidic conditions. We then assessed the biological and biophysical characteristics of pGlu-SC35EK-Hsl and its biostability in mouse serum.

2. Results and discussion

2.1. Cleavage and cyclization of the model synthetic peptide

In order to obtain the end-capped SC35EK protein, we incorporated two Met-Gln dipeptide cleavage sites across the anti-HIV SC35EK sequence. A CNBr-mediated cleavage should provide a C-terminal Hsl residue and an N-terminal Gln residue, which could then be converted into pGlu under mildly acidic conditions. Using a model synthetic peptide Ac-MQ-WEEWDKK-MQ-OH (MQ-SC7EK-MQ) **1** derived from the N-terminal sequence of SC35EK, the acidic conditions for CNBr-mediated cleavage and cyclization were optimized (Scheme 1). The reaction products were analyzed using LC–MS and the yields of Gln-SC7EK-Hsl **2** and pGlu-SC7EK-Hsl **3** were calculated based upon the peak areas at 220 nm (Table 1). The pGlu formation was verified by the comparative analysis with the authentic sample obtained by chemical synthesis using pyroglutamic acid. CNBr-mediated cleavage of peptide **1** in the standard 70% formic acid (FA) solution yielded Gln-SC7EK-Hsl **2** without the oxidation of Met residues (entry 1). Significant Met oxidation, which disrupted the cleavage reaction, was observed under the other acidic conditions, including 30% FA, 0.1 N HCl, 0.1 M trifluoroacetic acid (TFA) and 0.1 N AcOH. This by-product formation was prevented by the addition of tris(2-carboxyethyl)phosphine (TCEP) (entries 2–5). Partial production of the expected pGlu derivative **3** was observed in all cases in which this cyanylation step was carried out. The second cyclization, from N-terminal Gln to pGlu, was completed within 2 h. However, when 0.1 N AcOH solution was used, the reaction was incomplete (Fig. 1). Small amounts of formylated by-product were obtained along with peptide **3** in 70% FA solution, but peptide **3** was produced in higher yield (entry 1).

2.2. Preparation of recombinant His-tagged fusion protein

We used the pET28a(+) vector to express a hexa-histidine tagged [His-tag, $(His)_6$]-fusion protein in *E. coli*. The MQ-SC35EK-MQ sequence, or the tandem M-(Q-SC35EK-M)$_3$-Q sequence was spliced into the *NdeI-XhoI* restriction site downstream of the His-tag. This tandem sequence contains three consecutive anti-HIV peptides with five conjunctive Met-Gln cleavage sites designed to efficiently provide multiple SC35EK peptides from a single protein. Constructs were transformed into the *E. coli* strain BL21 (DE3)-RIL and protein expression was induced by IPTG. The resulting proteins were purified by affinity chromatography using Ni^{2+}-nitrilotriacetate (Ni-NTA)-agarose resin, and the expected proteins were eluted with either a standard imidazole buffer or an acidic solution con-

Table 1
Cleavage and cyclization reactions of a model synthetic peptide, MQ-SC7EK-MQ **1**, under acidic conditions

Entry	Solvent	Additive	Yield by CNBr treatment[a,c] (%)		Yield of pGlu formation[b,c] (%)	
			2	**3**	**2**	**3**
1	70% FA	–	78.3	2.4	–	70.7
2	30% FA	TCEP	60.5	5.7	–	57.7
3	0.1 N HCl	TCEP	63.8	5.8	4.5	61.2
4	0.1 M TFA	TCEP	62.7	6.5	3.5	60.1
5	0.1 N AcOH	TCEP	53.9	3.6	16.9	37.0

[a] CNBr treatment (100 equiv) was carried out for 2 h at room temperature.
[b] All cyclizations were carried out for 2 h at 60 °C.
[c] The yields were calculated based on the combined peak areas of the peptides at 220 nm after HPLC.

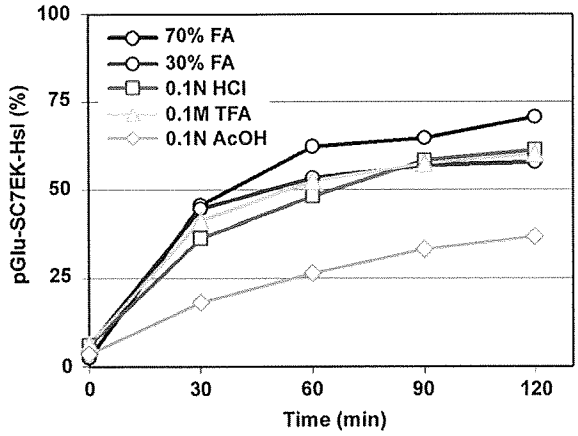

Figure 1. Time course of the cyclization process from Gln-SC7EK-Hsl to pGlu-SC7EK-Hsl. Cyclization of Gln to pGlu by heating the reaction at 60 °C under acidic conditions was monitored every 30 min for 2 h. The yields were calculated based on the combined peak areas at 220 nm of HPLC.

taining 70% FA, 0.1 N HCl or 0.1 M TFA. After elution using imidazole, the remaining imidazole was removed by gel-filtration. The sizes of the $(His)_6$-MQ-SC35EK-MQ **4** or $(His)_6$-M-(Q-SC35EK-M)$_3$-Q **5** fusion proteins on SDS–PAGE gels were 7.0 and 16.5 kDa, respectively (Fig. 2).

The $(His)_6$-MQ-SC35EK-MQ protein **4** was highly expressed in the soluble fraction and was obtained by elution with either imidazole or above acidic solutions from the affinity chromatography resin (Fig. 2a). Using the standard imidazole protocol, protein **4** was eluted in a moderate yield, however, approximately 100 mg of **4** was recovered from 1 L of bacterial culture under acidic solutions (Table 2). The lower yield obtained after elution using imidazole may be attributable either to incomplete protein elution from the column and/or protein loss during the desalting process. The purity of the $(His)_6$-MQ-SC35EK-MQ **4** was confirmed as >95% by HPLC (Fig. 4a). $(His)_6$-M-(Q-SC35EK-M)$_3$-Q **5** was expressed in both the soluble and insoluble fractions (Fig. 2b) and this resulted in a decreased yield, regardless of the high expression level seen in the total fraction. Consequently, only 19 or 26 mg/L of protein **5** was obtained by elution with imidazole or acidic solutions, respectively, (including 70% FA, 0.1 N HCl, or 0.1 M TFA), with <80% purity confirmed by HPLC. Thus, $(His)_6$-MQ-SC35EK-MQ **4** was used for the further experiments.

2.3. Production of the anti-HIV peptide by cleavage and cyclization of the recombinant protein

The optimized cleavage protocol established above was applied to $(His)_6$-MQ-SC35EK-MQ **4**. Purified protein **4** was cleaved and cyclized simultaneously by CNBr treatment under acidic conditions at 60 °C for 2 h (Scheme 2, and Fig. 3). All the LC–MS profiles indicated the formation of two major products corresponding to the tag fragment **6** and pGlu-SC35EK-Hsl **7** (Fig. 4b, top). The formylated by-products of **6** and **7** were only obtained by reaction in 70% FA. This result agrees with that obtained using the model peptide, and also with previous reports.[15b] Significant amounts of ring-opened products at the C-terminal Hsl of **6** and **7** were observed when the cleavage reaction was carried out in either 0.1 N HCl or 0.1 M TFA (Fig. 4b, middle and bottom). pGlu-SC35EK-Hsl **7** obtained under all conditions was purified by HPLC with >99% purity (Fig. 4c). Peptide **7** was characterized by ESI-MS measurement and by the comparative analysis with the one obtained by chemical synthesis using pGlu (see Supplementary data). The cyclization yields of pGlu-SC35EK-Hsl **7** obtained from the reaction in 70% FA, 0.1 N HCl, or 0.1 M TFA solutions were 16%, 15%, and 14%,

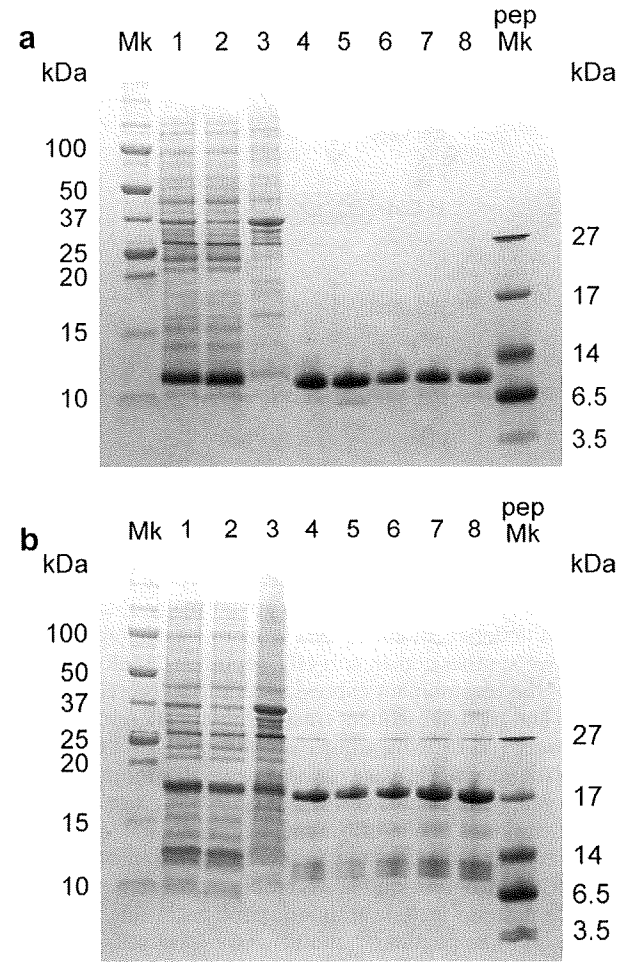

Figure 2. SDS–PAGE of recombinant proteins: (a) $(His)_6$-MQ-SC35EK-MQ **4** (7.0 kDa) and (b) $(His)_6$-M-(Q-SC35EK-M)$_3$-Q **5** (16.5 kDa). Lane Mk: molecular weight markers; lane 1: whole cell lysate; lane 2: supernatant of cell lysate; lane 3: precipitation of cell lysate; lane 4: pre-eluted resin; lanes 5–8: purified fractions from imidazole solution, 70% FA, 0.1 N HCl or 0.1 M TFA, respectively; lane pep Mk: polypeptide molecular weight markers.

respectively, and the overall yields from 1 L of *E. coli* culture were 10.4 mg, 10.2 mg, and 8.7 mg, respectively (Table 2).

2.4. Analysis of the SC35EK analog with end-capping groups by circular dichroism

The peptide conformation of pGlu-SC35EK-Hsl **7** was evaluated by measurement of the CD spectrum, along with SC35EK **8** and the non-end-capped peptide **9** (Fig. 5a, Table 3).[19] SC35EK **8** exhibits an α-helical conformation and interacts directly with an NHR-derived peptide, N36.[8a] The similar spectra with two characteristic spectrum minima at 208 and 222 nm were observed for peptides **7** and **8**. Peptide **9** showed significantly less α-helix formation compared with the other peptides, suggesting that the improved α-helical conformation of SC35EK is affected by the presence of the capping groups, but not by their structure. Potential six-helical bundle structure formation consisting of SC35EK derivatives **7**–**9** and N36, and the stability of the peptides, were also evaluated using CD analysis. The similar, stabilized α-helix conformations were verified within three complexes of six-helical bundle structures by the CD spectra (Fig. 5b). However, the thermal stability of the peptide **9**-N36 was less than those of the other two complexes [T_m(**7**) = 73.6 °C; T_m(**8**) = 75.8 °C; T_m(**9**) = 62.5 °C] (Fig. 5c and Table 3).

Table 2
Purification of proteins **4** and **5** by affinity chromatography and the subsequent CNBr-mediated cleavage and cyclization reactions of **4**

Entry	Solvent	Protein yield from 1 L culture[a] (mg)		Cyclization yield of **7** from **4** (%)[b,c]	Overall yield from 1 L culture of **4**[d] (mg)
		4	**5**		
1	Imidazole	35	19	–[e]	–[e]
2	70% FA	92	26	16	10.4
3	0.1 N HCl	100	26	15	10.2
4	0.1 M TFA	94	26	14	8.7

[a] The yield was quantified using Bradford protein assay.
[b] CNBr treatment (100 equiv) and cyclization were carried out for 2 h at 60 °C.
[c] The yield was quantified by UV absorbance at 280 nm.
[d] Peptide yields (mg) from 1 L culture of **4**.
[e] Not tested.

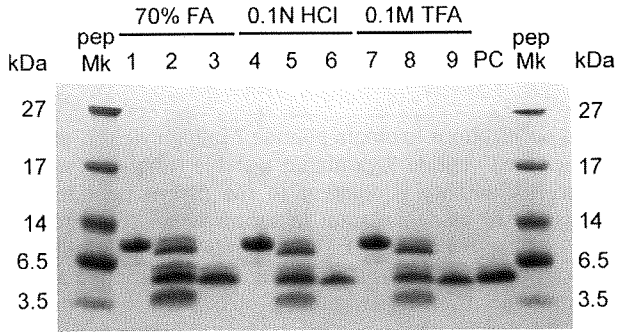

Figure 3. SDS-PAGE analysis of cleavage products and purified proteins. Lane Mk: polypeptide molecular weight marker; lanes 1, 4 and 7: $(His)_6$-MQ-SC35EK-MQ **4** (7.0 kDa); lanes 2, 5 and 8: after CNBr-mediated cleavage; lanes 3, 6 and 9: after HPLC purification; lane PC: chemically synthesized pGlu-SC35EK-Hsl **7** (control).

2.5. Anti-HIV activity

The anti-HIV activity of the SC35EK-derived peptides was evaluated using the MAGI assay (Table 3). pGlu-SC35EK-Hsl **7** reproduced the anti-HIV activity of SC35EK **8** [EC_{50}(**7**) = 0.57 nM; EC_{50}(**8**) = 0.50 nM], indicating that the original anti-HIV activity is not disrupted by the presence of the N- and C-terminal end-capping functional groups derived from the Met-Gln cleavage sites. The fivefold reduction in anti-HIV activity exhibited by peptide **9** compared with two other peptides was consistent with the less stable α-helix structures, both in the peptide itself and in the six-helical bundle complex.

2.6. Stability of the end-capped peptide in mouse serum

The ability of the N- and C-terminal capping moieties to protect the SC35EK analog **7** from biodegradation was assessed by incubating the peptides in mouse serum (Fig. 6). Rapid degradation of the non-end-capped peptide **9** was observed. Although pGlu-SC35EK-Hsl **7** was more stable than peptide **9**, ring-opening of the C-terminal Hsl in this peptide, followed by degradation at the C-terminus was observed.[20] This suggests that the pGlu end-capping group is

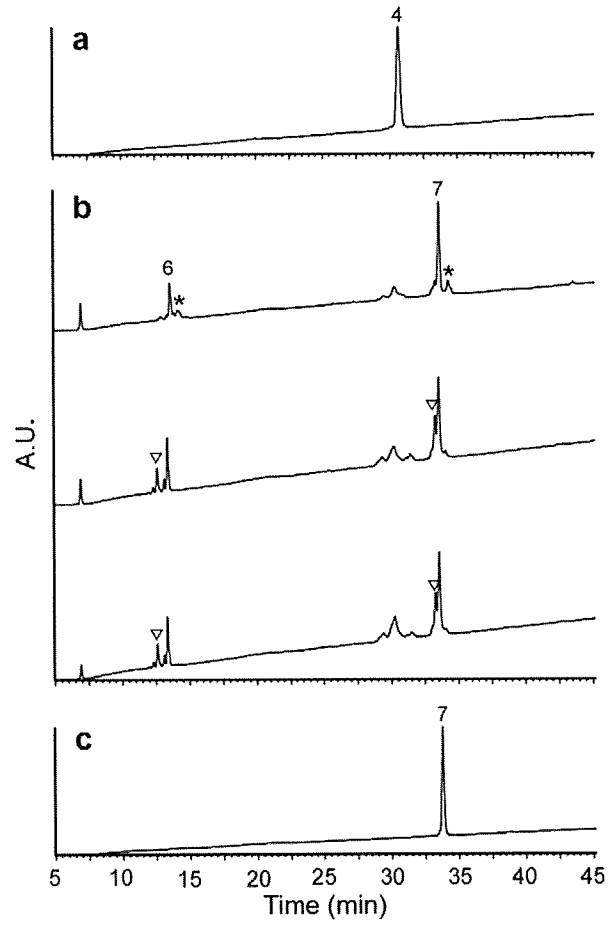

Figure 4. HPLC profiles of (a) $(His)_6$-MQ-SC35EK-MQ protein **4**; (b) the products of CNBr-mediated cleavage in (top) 70% FA, (middle) 0.1 N HCl, (bottom) 0.1 M TFA; (c) purified peptide **7**. Asterisk indicates the mono-formylated products of **6** and **7**. Inverted triangle indicates the ring-opened products at the Hsl of **6** and **7**. *HPLC conditions*: linear gradient 10–60% solvent B in solvent A over 50 min.

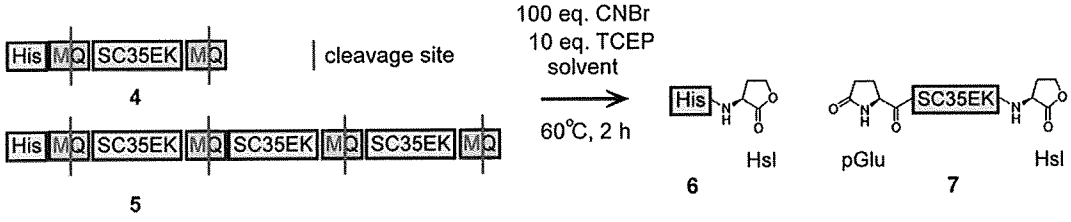

Scheme 2.

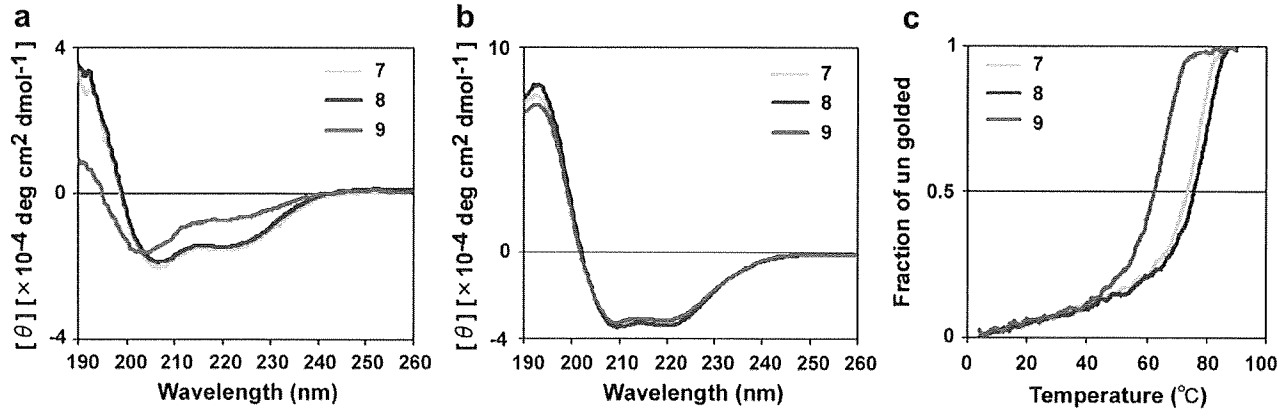

Figure 5. Secondary structure analysis using CD spectroscopy: CD spectra of (a) SC35EK-derived peptide; (b) SC35EK analog-N36 complex; and (c) thermostability of the SC35EK analog-N36 complex.

Table 3
Structures and anti-HIV activity of peptides **7–9**

Peptide	R^1	R^2	EC_{50}[a] (nM)	T_m (°C)
7	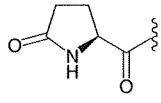	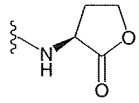	0.57 ± 0.24	73.6
SC35EK **8**	Ac	NH_2	0.50 ± 0.16	75.8
9	H	OH	2.43 ± 0.22	62.5

[a] EC_{50} was determined as the concentration that blocked HIV-1 infection by 50% in the MAGI assay.

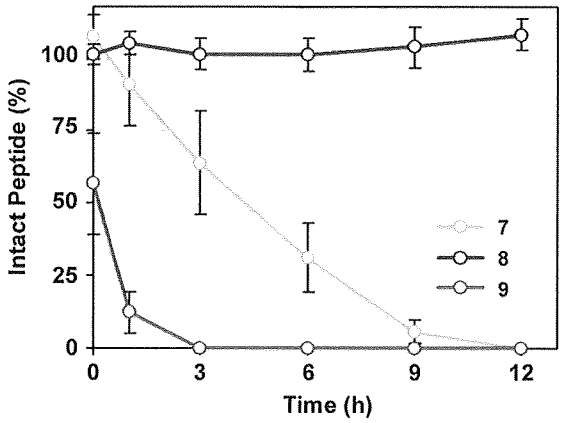

Figure 6. Degradation profile of peptides **7–9** by mouse serum. Each bar shows the mean ± SD ($n = 5$).

able to provide protection equivalent to that of an N-terminal acyl group. The γ-lactone structure of the C-terminal Hsl may be unfavorable for in vivo biostability compared with the C-terminal amide of peptide **8**, although the structure did not affect the in vitro anti-HIV activity.

3. Conclusions

The bioorganic synthesis of an end-capped anti-HIV peptide was achieved. The CNBr-mediated cleavages at the Met-Gln dipeptide sites of recombinant protein **4** afforded the end-capped SC35EK analog **7** bearing an N-terminal pGlu residue and a C-terminal Hsl residue. The acidic solution used for elution from the affinity chromatography resin to obtain the purified recombinant protein was also used for the cleavage-cyclization reactions. This facilitated the synthetic process and removed the need for repeated purifications to obtain peptide **7** in high yield. The resulting end-capped peptide **7** exhibited a stable α-helical conformation, anti-HIV activity equipotent to the parent peptide **8** and was resistant to biodegradation in serum when compared with the non-end-capped peptide **9**. The methods outlined in this paper are directly applicable to the preparation of end-capped anti-HIV fusion inhibitors from recombinant proteins, which may provide the next generation of therapeutic molecules active against multi-drug resistant strains of HIV-1.

4. Experimental

4.1. General

For HPLC separations of synthetic peptides, a Cosmosil 5C18-ARII analytical column (4.6 × 250 mm, flow rate 1 mL/min, Nacalai Tesque, Kyoto, Japan) or a Cosmosil 5C18-ARII preparative column (20 × 250 mm, flow rate 10 mL/min) was employed. The eluting products were detected by UV at 220 nm. A solvent system consisting of 0.1% TFA solution (v/v, solvent A) and 0.1% TFA in MeCN (v/v, solvent B) were used for HPLC elution.

4.2. Peptide synthesis

Protected peptide-resins were manually constructed by standard Fmoc-based SPPS on Rink amide resin (Novabiochem, 83 mg, 0.05 mmol). *t*-Bu for Tyr, Ser and Thr; *t*-Bu ester for Asp and Glu; Boc for Lys; and Trt for Asn and Gln were employed for side-chain protection, respectively. Fmoc-amino acids were coupled using five equivalents of reagents [Fmoc-amino acid, *N*,*N*′-diisopropylcarbodiimide and HOBt·H_2O] to free amino group in DMF for 1.5 h. Fmoc deprotection was performed by 20% piperidine in DMF (2 × 1 min, 1 × 20 min). The resulting protected resin was treated with TFA/H_2O/*m*-cresol/thioanisole/1,2-ethandithiol (80:5:5:5:5) at room temperature for 2 h. After removal of the resin by filtration, ice-cold dry Et_2O (30 mL) was added to the residue. The resulting powder was collected by centrifugation and then washed with ice-cold dry Et_2O (3 × 15 mL). Purification of the crude product by preparative HPLC afforded a colorless powder of the desired peptide. All peptides were characterized by an ESI-MS (micromassZQ2000, Waters), and the purity was calculated as >95% by HPLC.

4.3. Cleavage and cyclization of the model peptide

The model synthetic peptide MQ-SC7EK-MQ **1** was treated with CNBr (100 equiv) in the presence of TCEP (10 equiv) under acidic

conditions at room temperature for 2 h. After cleavage at the Met residue, the reaction mixture was heated at 60 °C for 2 h. The reaction products were analyzed every 30 min using LC–MS (Fig. 1). The Gln-SC7EK-Hsl **2** or the pGlu-SC7EK-Hsl **3** peptides were quantified based on the combined peak areas at 220 nm of peptides after HPLC.

4.4. Preparation of recombinant $(His)_6$-fused proteins

The cDNA sequences encoding the MQ-SC35EK-MQ or M-(Q-SC35EK-M)$_3$-Q proteins were amplified by PCR using the following chemically synthesized 139-mer or 361-mer oligonucleotides, respectively:

5′-ctc**CATATG**CAGTGGGAAGAATGGGATAAAAAAATTGAAGA
ATATACCAAAAAAATTGAAGAACTGATTAAAAAATCGGAAGAACAGCA
AAAAAAAAATGAAGAAGAACTGAAAAAAATGCAGTAA**CTCGAG**cgtt-3′

(both end of sequences in small letters indicate a flanking sequence for efficient restriction enzyme digestion of *Nde*I (CATATG) and *Xho*I (CTCGAG)) or 5′-ctc**GGATCCCATATG**CAGTGGGAGGAATGGGA
TAAAAAAATCGAAGAATATACTAAGAAAATTGAAGAACTCATCAAGAA
ATCCGAAGAACAACAGAAGAAAAACGAAGAGGAACTGAAAAAAATGC
AATGGGAAGAGTGGGACAAAAAGATCGAAGAGTATACCAAAAAAATC
GAAGAGTTGATTAAAAAGAGCGAAGAGCAGCAGAAAAAGAATGAAGA
AGAGTTAAAAAAGATGCAGTGGGAAGAATGGGACAAGAAAATTGAGG
AATACACTAAAAAGATCGAGGAACTGATTAAAAAATCTGAGGAACAGC
AGAAAAAAAATGAGGAAGAATTGAAGAAAATGCAATAA**CTCGAG**cgtt-3′

(both end of sequences in small letters indicate a flanking sequence for efficient restriction enzyme digestion of *Bam*HI (GGATCC), *Nde*I (CATATG) and *Xho*I (CTCGAG)).

Codons were replaced by more frequently used ones based on *E. coli* codon usage. The synthetic cDNA fragments contained *Nde*I and *Xho*I restriction sites at the 5′ and 3′ ends, respectively, and an extra ATGCAG or ATGCAA sequence (encoding Met-Gln, *underlined*) at their 5′ and 3′ termini across the SC35EK sequence to facilitate cleavage and cyclization. Each segment was digested with *Nde*I and *Xho*I and inserted into the pET28a (+) vector (Novagen). The plasmids [pET28a-MQ-SC35EK-MQ or pET28a-M(Q-SC35EK-M)$_3$-Q] were then transformed into the *E. coli* strain BL21(DE3)-RIL (Stratagene) for expression. Isolated colonies were picked and cultured overnight in 10 mL of LB culture containing 0.100 mg/mL kanamycin at 30 °C, with shaking. This culture was then transferred into 1 L of LB culture in the presence of 0.100 mg/mL kanamycin. When the OD_{600} reached 0.6–0.8, protein expression was initiated by the addition of 1 mM IPTG. After an additional 6-h incubation at 25 °C, the cells were harvested by centrifugation at 4000 rpm for 30 min. Cells were resuspended in B-PER solution (PIERCE) and disrupted by sonication. After centrifugation at 12,000 rpm for 30 min, the supernatant was transferred to a Ni-NTA agarose column (QIAGEN). The column was washed with wash buffer (20 mM phosphate, pH 6.0, containing 0.5 M NaCl) and the protein eluted with imidazole buffer (50–200 mM imidazole in phosphate buffer (pH 6.0)), 70% FA, 0.1 N HCl or 0.1 M TFA. The expression and purification of the proteins was analyzed by SDS–PAGE (15–20% gradient gel). The protein eluted with imidazole buffer was desalted by gel-filtration and freeze-dried. The freeze-dried protein was reconstituted in water to a concentration of 1 mM. The yield of the eluted proteins was calculated using a Protein Assay Kit (BIO-RAD Laboratories, Hercules, CA).

4.5. Preparation of the end-capped anti-HIV peptide from the recombinant protein

The protein eluted with an acidic solution was reconstituted to a concentration of 1 mM. The protein was treated with CNBr (100 equiv) in the presence of TCEP (10 equiv) under acidic conditions (as shown in Table 2) at 60 °C for 2 h and the products were analyzed by LC–MS. Preparative HPLC of the product provided the expected end-capped peptide. The yield of purified peptide was calculated by measuring the UV absorbance at 280 nm.

4.6. Measurement of CD spectra

Peptides **7–9** were dissolved in 5 mM HEPES buffer (pH 7.2) to a final concentration of 10 μM. For CD measurement of a mixture of the NHR peptide (N36) and SC35EK analogs, the peptides were incubated at 37 °C for 30 min beforehand. The wavelength-dependent molar ellipticity $[\theta]$ was monitored at 25 °C as the average of 8 scans in a Jasco spectropolarimeter (Model J-710, Jasco Inc., Tokyo, Japan). Thermal unfolding of the potential six-helical bundle in the presence of N36 was monitored by the $[\theta]_{222}$ values at intervals of 0.5 °C after a 15-s equilibration at the desired temperature and an integration time of 1.0 s. The midpoint of the thermal unfolding transition of each complex was defined as the melting temperature (T_m).

4.7. Determination of drug susceptibility of HIV-1

The peptide sensitivity of infectious clones was determined by the MAGI assay with some modifications.[21] Briefly, the target cells (HeLa-CD4/CCR5-LTR-β-gal; 10^4 cells/well) were plated in 96-well flat microtiter culture plates. On the following day, the cells were inoculated with the HIV-1 clone (NL4-3, 60 MAGI U/well, giving 60 blue cells after 48 h of incubation) and cultured in the presence of various concentrations of drugs in fresh medium. After (48 h) viral exposure, all the blue cells stained with X-Gal (5-bromo-4-chloro-3-indolyl-β-D-galactopyranoside) were counted in each well. The activity of test compounds was determined as the concentration that blocked HIV-1 replication by 50% (50% effective concentration [EC_{50}]).

4.8. Stability of SC35EK peptide or analogs in mouse serum

Peptides **7–9** (0.5 mM in PBS) were incubated at 37 °C in 50% mouse serum in the presence of 0.1% *m*-cresol (internal standard). 0.010 mL samples were collected at 0, 0.5, 1, 3, 6, 9 and 12 h and the reaction was terminated by the addition of 1 μL 0.1 N HCl and 0.040 mL of CH_3CN. Samples were deproteinized by centrifugation at 12,000 rpm for 10 min and 0.010 mL of the supernatant was injected into LC–MS. The percentage of intact peptides was calculated by peak area and corrected against the internal standard.

Acknowledgements

This work was supported by Science and Technology Incubation Program in Advanced Regions from Japan Science and Technology Agency, and Health and Labour Sciences Research Grants (Research on HIV/AIDS).

Supplementary data

Supplementary data associated with this article can be found, in the online version, at doi:10.1016/j.bmc.2009.10.017.

References and notes

1. Richman, D. D.; Morton, S. C.; Wrin, T.; Hellmann, N.; Berry, S.; Shapiro, M. F.; Bozzette, S. A. *AIDS* **2004**, *18*, 1393.
2. For a review, see: Flexner, C. *Nat. Rev. Drug Disc.* **2007**, *6*, 959.
3. Chan, D. C.; Kim, P. S. *Cell* **1998**, *93*, 981.
4. Eckert, D. M.; Kim, P. S. *Annu. Rev. Biochem.* **2001**, *70*, 777.
5. (a) Wild, C.; Oas, T.; McDanal, C.; Bolognesi, D.; Matthews, T. *Proc. Natl. Acad. Sci. U.S.A.* **1992**, *89*, 10537; (b) Wild, C.; Greenwell, T.; Matthews, T. *AIDS Res.*

Hum. Retroviruses **1993**, *9*, 1051; (c) Wild, C. T.; Shugars, D. C.; Greenwell, T. K.; McDanal, C. B.; Matthews, T. J. *Proc. Natl. Acad. Sci. U.S.A.* **1994**, *91*, 9770.
6. For a review, see: Matthews, T.; Salgo, M.; Greenberg, M.; Chung, J.; DeMasi, R.; Bolognesi, D. *Nat. Rev. Drug Disc.* **2004**, *3*, 215.
7. (a) Izumi, K.; Kodama, E.; Shimura, K.; Sakagami, Y.; Watanabe, K.; Ito, S.; Watabe, T.; Terakawa, Y.; Nishikawa, H.; Sarafianos, S. G.; Kitaura, K.; Oishi, S.; Fujii, N.; Matsuoka, M. *J. Biol. Chem.* **2009**, *284*, 4914; (b) Watabe, T.; Terakawa, Y.; Watanabe, K.; Ohno, H.; Nakano, H.; Nakatsu, T.; Kato, H.; Izumi, K.; Kodama, E.; Matsuoka, M.; Kitaura, K.; Oishi, S.; Fujii, N. *J. Mol. Biol.* **2009**, *392*, 657.
8. (a) Otaka, A.; Nakamura, M.; Nameki, D.; Kodama, E.; Uchiyama, S.; Nakamura, S.; Nakano, H.; Tamamura, H.; Kobayashi, Y.; Matsuoka, M.; Fujii, N. *Angew. Chem., Int. Ed.* **2002**, *41*, 2937; (b) Oishi, S.; Ito, S.; Nishikawa, H.; Watanabe, K.; Tanaka, M.; Ohno, H.; Izumi, K.; Sakagami, Y.; Kodama, E.; Matsuoka, M.; Fujii, N. *J. Med. Chem.* **2008**, *51*, 388; (c) Nishikawa, H.; Oishi, S.; Fujita, M.; Watanabe, K.; Tokiwa, R.; Ohno, H.; Kodama, E.; Izumi, K.; Kajiwara, K.; Naitoh, T.; Matsuoka, M.; Otaka, A.; Fujii, N. *Bioorg. Med. Chem.* **2008**, *16*, 9184; (d) Nishikawa, H.; Nakamura, S.; Kodama, E.; Ito, S.; Kajiwara, K.; Izumi, K.; Sakagami, Y.; Oishi, S.; Ohkubo, T.; Kobayashi, Y.; Otaka, A.; Fujii, N.; Matsuoka, M. *Int. J. Biochem. Cell Biol.* **2009**, *41*, 891; (e) Naito, T.; Izumi, K.; Kodama, E.; Sakagami, Y.; Kajiwara, K.; Nishikawa, H.; Watanabe, K.; Sarafianos, S. G.; Oishi, S.; Fujii, N.; Matsuoka, M. *Antimicrob. Agents Chemother.* **2009**, *53*, 1013.
9. Bray, B. L. *Nat. Rev. Drug Disc.* **2003**, *2*, 587.
10. Dingermann, T. *Biotechnol. J.* **2008**, *3*, 90.
11. (a) Rao, X. C.; Li, S.; Hu, J. C.; Jin, X. L.; Hu, X. M.; Huang, J. J.; Chen, Z. J.; Zhu, J. M.; Hu, F. Q. *Protein Expr. Purif.* **2004**, *36*, 11; (b) Park, T. J.; Kim, J. S.; Choi, S. S.; Kim, Y. *Protein Expr. Purif.* **2009**, *65*, 23; (c) Zorko, M.; Japelj, B.; Hafner-Bratkovic, I.; Jerala, R. *Biochim. Biophys. Acta* **2009**, *1788*, 314.
12. Zhao, D. X.; Ding, Z. C.; Liu, Y. Q.; Huang, Z. X. *Protein Expr. Purif.* **2007**, *53*, 232.
13. Chang, S. G.; Kim, D. Y.; Choi, K. D.; Shin, J. M.; Shin, H. C. *Biochem. J.* **1998**, *329*, 631.
14. Riley, J. M.; Aggeli, A.; Koopmans, R. J.; McPherson, M. J. *Biotechnol. Bioeng.* **2009**, *103*, 241.
15. (a) Gross, E.; Witkop, B. *J. Biol. Chem.* **1962**, *237*, 1856; (b) Kaiser, R.; Metzka, L. *Anal. Biochem.* **1999**, *266*, 1.
16. Abraham, G. N.; Podell, D. N. *Mol. Cell. Biochem.* **1981**, *38*, 181.
17. (a) Schilling, S.; Hoffmann, T.; Rosche, F.; Manhart, S.; Wasternack, C.; Demuth, H. U. *Biochemistry* **2002**, *41*, 10849; (b) Fernández, G. A.; Butz, P.; Trierweiler, B.; Zöller, H.; Stärke, J.; Pfaff, E.; Tauscher, B. *J. Agric. Food Chem.* **2003**, *51*, 8093; (c) Chelius, D.; Jing, K.; Lueras, A.; Rehder, D. S.; Dillon, T. M.; Vizel, A.; Rajan, R. S.; Li, T.; Treuheit, M. J.; Bondarenko, P. V. *Anal. Chem.* **2006**, *78*, 2370.
18. Recently, we have reported the preparation of HIV fusion inhibitor SC34EK by an alternative cleavage reaction using 1-cyano-4-dimethylaminopyridinium tetrafluoroborate (CDAP) for the Cys residues: Tanaka, M.; Kajiwara, K.; Tokiwa, R.; Watanabe, K.; Ohno, H.; Tsutsumi, H.; Hata, Y.; Izumi, K.; Kodama, E.; Matsuoka, M.; Oishi, S.; Fujii, N. *Bioorg. Med. Chem.* **2009**, *17*, 7487.
19. Non-end capped peptide **9** can be obtained by standard recombinant expression in prokaryotes. Peptide **9** for this experiment was obtained by the chemical synthesis.
20. The ring-opening C-terminal Hsl was verified by the observed +18 mass of the product, supporting the presence of Hsl in peptide **7**.[15] The ring-opened product may be degraded from the C-terminus by endopeptidases in serum.
21. (a) Maeda, Y.; Venzon, D. J.; Mitsuya, H. *J. Infect. Dis.* **1998**, *177*, 1207; (b) Kodama, E. I.; Kohgo, S.; Kitano, K.; Machida, H.; Gatanaga, H.; Shigeta, S.; Matsuoka, M.; Ohrui, H.; Mitsuya, H. *Antimicrob. Agents Chemother.* **2001**, *45*, 1539.

THE JOURNAL OF BIOLOGICAL CHEMISTRY VOL. 284, NO. 51, pp. 35681–35691, December 18, 2009
Printed in the U.S.A.

Mechanism of Inhibition of HIV-1 Reverse Transcriptase by 4′-Ethynyl-2-fluoro-2′-deoxyadenosine Triphosphate, a Translocation-defective Reverse Transcriptase Inhibitor*

Received for publication, June 23, 2009, and in revised form, October 14, 2009 Published, JBC Papers in Press, October 16, 2009, DOI 10.1074/jbc.M109.036616

Eleftherios Michailidis[‡], Bruno Marchand[‡1], Eiichi N. Kodama[§2], Kamlendra Singh[‡], Masao Matsuoka[§], Karen A. Kirby[‡], Emily M. Ryan[‡], Ali M. Sawani[‡], Eva Nagy[¶], Noriyuki Ashida[‖], Hiroaki Mitsuya[‡‡], Michael A. Parniak[¶], and Stefan G. Sarafianos[‡3]**

From the [‡]Christopher Bond Life Sciences Center, Department of Molecular Microbiology and Immunology, University of Missouri, Columbia, Missouri 65211, the [§]Institute for Virus Research, Kyoto University, Kyoto 606-8507, Japan, the [¶]Department of Molecular Genetics and Biochemistry, University of Pittsburgh, Pittsburgh, Pennsylvania 15261, [‖]Yamasa Corporation, Chiba 288-0056, Japan, the [**]Department of Hematology and Infectious Diseases, Kumamoto University, Kumamoto 860-8556, Japan, and the [‡‡]Experimental Retrovirology Section, HIV/AIDS Malignancy Branch, National Institutes of Health, Bethesda, Maryland 20892

Nucleoside reverse transcriptase inhibitors (NRTIs) are employed in first line therapies for the treatment of human immunodeficiency virus (HIV) infection. They generally lack a 3′-hydroxyl group, and thus when incorporated into the nascent DNA they prevent further elongation. In this report we show that 4′-ethynyl-2-fluoro-2′-deoxyadenosine (EFdA), a nucleoside analog that retains a 3′-hydroxyl moiety, inhibited HIV-1 replication in activated peripheral blood mononuclear cells with an EC_{50} of 0.05 nM, a potency several orders of magnitude better than any of the current clinically used NRTIs. This exceptional antiviral activity stems in part from a mechanism of action that is different from approved NRTIs. Reverse transcriptase (RT) can use EFdA-5′-triphosphate (EFdA-TP) as a substrate more efficiently than the natural substrate, dATP. Importantly, despite the presence of a 3′-hydroxyl, the incorporated EFdA monophosphate (EFdA-MP) acted mainly as a *de facto* terminator of further RT-catalyzed DNA synthesis because of the difficulty of RT translocation on the nucleic acid primer possessing 3′-terminal EFdA-MP. EFdA-TP is thus a translocation-defective RT inhibitor (TDRTI). This diminished translocation kept the primer 3′-terminal EFdA-MP ideally located to undergo phosphorolytic excision. However, net phosphorolysis was not substantially increased, because of the apparently facile reincorporation of the newly excised EFdA-TP. Our molecular modeling studies suggest that the 4′-ethynyl fits into a hydrophobic pocket defined by RT residues Ala-114, Tyr-115, Phe-160, and Met-184 and the aliphatic chain of Asp-185. These interactions, which contribute to both enhanced RT utilization of EFdA-TP and difficulty in the translocation of 3′-terminal EFdA-MP primers, underlie the mechanism of action of this potent antiviral nucleoside.

Nucleoside reverse transcriptase inhibitors (NRTIs)[4] are central components of first line regimens for treatment of HIV infections (1–6). Currently, there are eight clinically approved NRTIs: AZT, 3TC, FTC, ABC, ddI, ddC, d4T, and the nucleotide tenofovir (TFV; reviewed in Refs. 7 and 8). A structural hallmark of these NRTIs is the lack of a 3′-OH; it has long been considered that the absence of the 3′-OH is essential for antiviral activity. However, the absence of the 3′-OH in NRTIs also imparts detrimental properties to the inhibitor, including reduced affinity for RT compared with the analogous dNTP substrate, as well as reduced intracellular conversion to the active nucleoside triphosphate (9).

Previously we described a series of 4′-substituted NRTIs (10) that retain the 3′-OH group and have excellent antiviral properties and significantly improved selectivity indices (CC_{50}/EC_{50}) compared with the approved NRTIs. Furthermore, these NRTIs efficiently suppress various NRTI-resistant HIV. The most potent of these 4′-substituted NRTIs are the adenosine analogs that have an ethynyl group at the 4′ position of the ribose ring. Despite their high anti-HIV activity, 4′-substituted compounds are susceptible to degradation by adenosine deaminase (11), a property that limits the plasma and intracellular half-life of the drugs. To overcome the adenosine deaminase sensitivity of these 4′-ethynyl NRTIs, we developed a second generation of analogs substituted at the 2-position of the adenine ring (12). We recently reported that the 2-halogenated, 4′-ethynyl compounds have remarkably improved potency and selectivity indices (CC_{50}/EC_{50}) compared with the nonhalogenated analogs and significantly better ones compared with

* This work was supported, in whole or in part, by National Institutes of Health Grants AI076119, AI074389, AI076119-S1, and AI076119-02S1 (to S. G. S.) and AI079801 (to M. A. P.).

[1] Recipient of the amfAR Mathilde Krim Fellowship.
[2] Present address: Div. of Emerging Infectious Diseases, Tohoku University School of Medicine, Sendai 980-8575, Japan.
[3] To whom correspondence should be addressed: 471d Christopher S. Bond Life Sciences Ctr., 1201 Rollins St., Columbia, MO 65211. Tel.: 573-882-4338; E-mail: sarafianoss@missouri.edu.

[4] The abbreviations used are: NRTI, nucleoside reverse transcriptase inhibitor; TDRTI, translocation-defective RT inhibitor; RT, reverse transcriptase; HIV, human immunodeficiency virus; EFdA, 4′-ethynyl-2-fluoro-2′-deoxyadenosine; MP, monophosphate; TP, triphosphate; AZT, azidothymidine; EdA, 4′-ethynyl-2′-deoxyadenosine; EFddA, 4′-ethynyl-2-fluoro-2′,3′-dideoxyadenosine; EFd4A, 4′-ethynyl-2-fluoro-2′,3′-dihydro-2′,3′-dideoxyadenosine; Ed4T, 4′-ethynyl-2′,3′-dihydro-3′-deoxythymidine; TFV, tenofovir; PBMC, peripheral blood mononuclear cell; T/P, template/primer; $T/P_{EFdA\text{-}MP}$ or $T/P_{ddA\text{-}MP}$, template/primer possessing either EFdA-MP or ddAMP at the 3′-primer terminus (or T/P chain terminated by EFdA or ddA); N-site, nucleotide-binding site; P-site, primer site; PDB, Protein Data Bank; d4T, stavudine.

TABLE 1

DNA and RNA sequences used in this study

The primers were fluorescently labeled at the 5′-end except for the footprinting experiments, in which the template was fluorescently labeled at the 5′-end.

Polymerization experiments	
T_{d100}	5′-TAG TGT GTG CCC GTC TGT TGT GTG ACT CTG GTA ACT AGA GAT CCC TCA GAC CCT TTT AGT CAG TGT GGA AAA TCT CTA GCA GTG GCG CCC GAA CAG GGA C
P_{d18}	5′-Cy3 GTC CCT GTT CGG GCG CCA
T_{d31}	5′-CCA TAG CTA GCA TTG GTG CTC GAA CAG TGA C
T_{r31}	5′-CCA UAG CUA GCA UUG GUG CUC GAA CAG UGA C
P_{d18}	5′-Cy3 GTC ACT GTT CGA GCA CCA
Gel shift experiments	
T_{d43}	5′-AAT CAG TGT AGA CAA TCC CTA GCA TTG GTG CTC GAA CAG TGA C
P_{d18}	5′-Cy3 GTC CCT GTT CGG GCG CCA
Footprinting experiments	
P_{d20}	5′-TTG TCA CTG TTC GAG CAC CA
T_{d43}	5′-Cy3 CCA TAG CTA GCA TTG GTG CTC GAA CAG TGA CAA TCA GTG TAGA

other approved NRTIs. These compounds are resistant to degradation by adenosine deamination (13). The most potent of these compounds is EFdA (Fig. 1*A*), which was recently shown not to inhibit human DNA polymerases α and β or mitochondrial DNA polymerase γ (12). Notably, clinically important drug-resistant HIVs (14, 15) are sensitive or hypersensitive to this compound (13).

Despite its remarkable antiviral potency, the molecular mechanism by which EFdA and related compounds inhibit HIV is unknown. To elucidate this mechanism we carried out biochemical experiments that systematically decipher the effect of EFdA on each of the mechanistic steps of DNA synthesis by HIV RT. On the basis of these experiments we propose that EFdA-5′-triphosphate (EFdA-TP) inhibits RT by first being incorporated at the 3′-primer terminus, and after its incorporation it prevents further addition of nucleotides by blocking the translocation of the primer strand on the viral polymerase. We therefore termed EFdA a "translocation-defective reverse transcriptase inhibitor (TDRTI)." By understanding the molecular details of RT inhibition by a highly potent NRTI, we hope to gain insights into the design of even more efficacious inhibitors that may act via same or similar mechanisms.

EXPERIMENTAL PROCEDURES

Enzymes and Nucleic Acids

The RT genes coding for p66 and p51 subunits of BH10 HIV-1 were cloned in the pETDuet-1 vector (Novagen) using restriction sites NcoI and SacI for the p51 subunit and SacII and AvrII for the p66 subunit. The sequences coding for a hexahistidine tag and the 3C protease recognition sequence were added at the N terminus of the p51 subunit. RT was expressed in BL21 (Invitrogen) and purified by nickel affinity chromatography and MonoQ anion exchange chromatography (16). Oligonucleotides used in this study were synthesized chemically and purchased from Integrated DNA Technologies (Coralville, IA). Sequences of the DNA/RNA substrates are shown in Table 1. Deoxynucleotide triphosphates and dideoxynucleotide triphosphates were purchased from Fermentas (Glen Burnie, MD). EFdA was synthesized by Yamasa Corp. (Chiba, Japan) as described previously (12). Using EFdA as the starting material, the triphosphate form, EFdA-TP, was synthesized by TriLink BioTechnologies (San Diego, CA). Concentrations of nucleotides and EFdA-TP were calculated spectrophotometrically on the basis of absorption at 260 nm and their extinction coefficients. All nucleotides were treated with inorganic pyrophosphatase (Roche Diagnostics) as described previously (17) to remove traces of PP_i contamination that might interfere with the rescue assay.

Cell-based HIV-1 Replication Assays

Peripheral blood mononuclear cells (PBMCs) were isolated from healthy donor buffy coats (purchased from the Central Blood Bank, Pittsburgh, PA) using Ficoll-Hypaque (Histopaque, Sigma-Aldrich) gradient centrifugation as described previously (18). PBMCs were stimulated with 5 μg/ml phytohemagglutinin (Sigma) in RPMI 1640 containing 10% fetal bovine serum for 48 h prior to exposure to drug and virus. After washing, the activated cells were resuspended in RPMI 1640/fetal bovine serum containing interleukin-2 (10 units/ml) and varying concentrations of the NRTIs and then were infected with HIV-1_{NL4-3} at a multiplicity of infection of 0.01. HIV-1 infection was assessed by measuring HIV-1 p24 antigen in cell-free culture supernatants obtained 7 days post-infection using an HIV-1 p24 antigen capture assay kit (SAIC, Frederick, MD).

Primer Extension Assays

Characterization of EFdA-TP as a Chain Terminator—DNA or RNA template was annealed to a 5′-Cy3-labeled DNA primer (3:1 molar ratio). To monitor the primer extension, the DNA/DNA or RNA/DNA hybrid (20 nM) was incubated at 37 °C with HIV-1 RT (20 nM) in a buffer containing 50 mM Tris (pH 7.8) and 50 mM NaCl (RT buffer). Subsequently, varying amounts of EFdA-TP or ddATP were added, and the reactions were initiated by the addition of 6 mM $MgCl_2$ to a final volume of 20 μl. All dNTPs were present at a final concentration of 1 μM. The reactions were terminated after 15 min by adding an equal volume of 100% formamide containing traces of bromphenol blue. The products were resolved on a 15% polyacrylamide 7 M urea gel. In this and subsequent assays, the gels were scanned with a phosphorimaging device (FLA 5000, FujiFilm). The bands for fully extended product were quantified using Multi Gauge software (FujiFilm), and the results were plotted as percent full extension using GraphPad Prism 4 to determine the IC_{50} for EFdA-TP and other nucleotide analogs.

Steady State Kinetics—Steady state kinetic parameters, K_m and k_{cat}, for incorporation of EFdA-MP or dAMP were determined using single nucleotide incorporation in gel-based assays under saturating substrate conditions. The reactions were car-

ried out in RT buffer with 6 mM $MgCl_2$, 100 nM T_{d31}/P_{d18} or T_{r31}/P_{d18}, and 2.5 nM RT in a final volume of 20 μl and stopped at the indicated reaction times. The products were resolved and quantified as described above. K_m and k_{cat} were determined graphically using the Michaelis-Menten equation.

Incorporation of dNTP to the Template/Primer (T/P) Possessing Either EFdA-MP ($T/P_{EFdA\text{-}MP}$) or ddAMP (T/P_{ddAMP}) at the 3′-Primer Terminus—$T/P_{EFdA\text{-}MP}$ and T/P_{ddAMP} were prepared by incubating 500 nM T_{d31}/P_{d18} with 1 μM HIV-1 RT in RT buffer and 6 mM $MgCl_2$. EFdA-TP (1 μM) or ddATP (5 μM) was added into the reaction and the mixture was incubated at 37 °C for 1 h. After incorporation of the nucleotide analogs, the T/P_{analog} was purified using the QIAquick nucleotide removal kit (Qiagen, Valencia, CA). Under these conditions, the extension of T/P to $T/P_{EFdA\text{-}MP}$ or T/P_{ddAMP} was complete. Purified $T/P_{EFdA\text{-}MP}$ (5 nM) was incubated with 20 nM HIV-1 RT in RT buffer and 6 mM $MgCl_2$. The first incoming nucleotide was added at different concentrations (0–100 μM) in the presence of the other dNTPs (1 μM). The reactions were incubated at 37 °C for 15 or 60 min.

Gel Mobility Shift Assays

Formation of RT·DNA Binary Complex—$T/P_{EFdA\text{-}MP}$ and T/P_{ddAMP} were prepared using T_{d43}/P_{d18} as described above. Purified $T/P_{EFdA\text{-}MP}$ or T/P_{ddAMP} (20 nM) was incubated at room temperature for 10 min with different concentrations of HIV-1 RT in RT buffer and 6 mM $MgCl_2$. RT was used at different concentrations to obtain RT/DNA ratios that ranged from 0.25 to 7.5. Four μl of 20% sucrose was added to each mixture in a final volume of 20 μl. The complexes were subsequently resolved on a native 6% polyacrylamide Tris borate gel and visualized as described above.

Formation of $RT{\cdot}DNA_{EFdA\text{-}MP}{\cdot}dTTP$ Ternary Complex—Purified $T/P_{EFdA\text{-}MP}$ or T/P_{ddAMP} (9 nM) was incubated at room temperature for 10 min with 100 nM HIV-1 RT, varying amounts of the next nucleotide (1–5000 μM) in RT buffer, and 6 mM $MgCl_2$. Prior to the addition of sucrose, 150 ng/μl heparin was added, and finally the products were resolved on native 6% polyacrylamide Tris borate gels and visualized as described above.

Site-specific Fe^{2+} Footprinting Assay

Site-specific Fe^{2+} footprints were monitored on 5′-Cy3-labeled DNA templates. T_{d43}/P_{d20} (100 nM) was incubated with HIV-1 RT (600 nM) in a buffer containing 120 mM sodium cacodylate (pH 7), 20 mM NaCl, 6 mM $MgCl_2$, and EFdA-TP (1 μM) to allow quantitative chain termination. Prior to treatment with Fe^{2+}, complexes were preincubated for 7 min with increasing concentrations of the next nucleotide as indicated in Fig. 5*A*. The complexes were treated with ammonium iron sulfate (1 mM) as described previously (19). This reaction relies on autoxidation of Fe^{2+} (20) to create a local concentration of the hydroxyl radical, which cleaves the DNA at the nucleotide closest to the Fe^{2+} specifically bound to the RNase H active site.

PP_i- and ATP-dependent Excision and Rescue of $T/P_{EFdA\text{-}MP}$ and T/P_{ddAMP}

PP_i-dependent Excision of $T/P_{EFdA\text{-}MP}$ and T/P_{ddAMP}—Purified $T/P_{EFdA\text{-}MP}$ and T/P_{ddAMP} (20 nM) were incubated at 37 °C with HIV-1 RT (60 nM) in the presence of 150 μM PP_i in RT buffer and 6 mM $MgCl_2$. Aliquots of the reaction were stopped at different times (0–30 min) and analyzed as described above.

PP_i-dependent Rescue of $T/P_{EFdA\text{-}MP}$ and T/P_{ddAMP}—Purified $T/P_{EFdA\text{-}MP}$ and T/P_{ddAMP} (20 nM) were incubated with HIV-1 RT (60 nM) at various concentrations of PP_i (0–150 μM) in RT buffer and 6 mM $MgCl_2$. The assay was performed in the presence of a large excess of competing dATP (100 μM), which prevented reincorporation of EFdA-MP, 0.5 μM dTTP, and 10 μM ddGTP. After an incubation of 10 min at 37 °C, the reactions were stopped and analyzed as described above.

ATP-dependent Rescue of $T/P_{EFdA\text{-}MP}$ and T/P_{ddAMP}—Purified $T/P_{EFdA\text{-}MP}$ and T/P_{ddAMP} (20 nM) were incubated with HIV-1 RT (60 nM) in the presence of 3.5 mM ATP, 100 μM dATP, 0.5 μM dTTP, and 10 μM ddGTP in RT buffer and 10 mM $MgCl_2$. Aliquots of the reaction were stopped at different time points (0–90 min) and analyzed as described above.

Molecular Modeling

Molecular models of two reaction intermediates that involve EFdA were built as follows. 1) A model of the ternary complex of HIV-1 RT·DNA·EFdA-TP (Fig. 7*A*) was built starting with the coordinates of the crystal structure of the HIV-1 RT·DNA·TFV-DP complex. The triphosphate of EFdA-TP was built using as a guide the corresponding atoms of TFV-DP in structure with PDB code 1T05 and of dTTP in PDB code 1RTD. The coordinates of the 4′-ethynyl sugar ring were from our NMR structure of EFdA[5] showing that EFdA is in a North conformation similar to the sugar puckering observed in the crystal structure of 4′-ethynyl-2′-deoxycytidine (21). The structure of the EFdA-TP was assembled from its components using the sketch module of Sybyl 7.0 (Tripos Associates, St. Louis, MO), and minimized by the semiempirical quantum chemical method PM3 (22). The PM3 charges and the docking module of Sybyl 7.0 were used to dock the EFdA-TP at the RT dNTP-binding site (after removing the TFV-DP from 1T05) to generate the ternary complex HIV-1 RT·T/P·EFdA-TP. The final complex structure was minimized for 100 cycles using the AMBER force field with Coleman united charges on the protein and DNA molecules. 2) The model of the $RT{\cdot}T/P_{EFdA\text{-}MP}$ binary complex with primer 3′-terminal EFdA-MP at the pre-translocation nucleotide-binding site (N-site) (or dNTP-binding site) (Fig. 7*B*) was built using as a starting model our crystal structure of the pre-translocation complex $RT{\cdot}T/P_{AZT\text{-}MP}$ (PDB code 1N6Q). The structures of AZTMP and the base-pairing dA were replaced by EFdA-MP (built as in EFdA-TP above) and a dT, respectively, using the sketch module of Sybyl 7.0, and energy-minimized using the AMBER force field with Coleman united charges on the protein and DNA molecules.

[5] K. A. Kirby, K. Singh, E. Michailidis, B. Marchand, E. N. Kodama, E. Nagy, N. Ashida, H. Mitsuya, M. A. Parniak, and S. G. Sarafianos, unpublished data.

RESULTS

EFdA-TP Is a Highly Potent Inhibitor of HIV-1 RT—EFdA inhibits HIV-1 replication in phytohemagglutinin-activated PBMCs with an EC_{50} of 50 pM (Table 2), consistent with previously published data obtained using T-cell lines (12, 13), and data published after completion of this work (23). The antiviral potency of EFdA is at least 4 orders of magnitude greater than the clinically used adenine nucleotide analog tenofovir and over 400-fold greater than that of AZT when assessed under the same conditions (Table 2). EFdA thus appears to be the most potent nucleoside inhibitor described to date of HIV-1 replication in primary cells. It is also interesting to note that EFdA is substantially more potent than analogs lacking a 3′-OH function (EFddA and EFd4A; Table 2). No cytotoxicity was noted at 10 μM EFdA (data not shown), the highest concentration tested, suggesting an *in vitro* selectivity index of over 200,000. To better understand the molecular basis for the exceptional antiviral potency of EFdA, we carried out a series of detailed *in vitro* evaluations of the impact of the active antiviral form of EFdA, namely EFdA-TP, on DNA synthesis catalyzed by purified HIV-1 RT.

TABLE 2
Inhibition of HIV-1 replication in phytohemagglutinin-activated PBMCs by EFdA, EFdA analogs, and other NRTIs

Compound	EC_{50}[a]
	nM
EFdA	0.05 ± 0.02
EdA	11 ± 7
EFddA	570 ± 92
EFd4A	14 ± 11
Zidovudine (or AZT)	22 ± 7
Tenofovir	3300 ± 1240

[a] Values are means ± S.D. of triplicate determinations and were determined by assessment of reduction in HIV-1 p24 antigen production in infected cells as described under "Experimental Procedures."

We first compared the effect of EFdA-TP with other NRTI-TPs (ddATP, TFV-DP, AZTTP, and ddCTP) on RT-catalyzed DNA synthesis in *in vitro* primer extension assays using a nucleic acid T/P comprising a 100-nucleotide DNA template annealed to a Cy3–5′-labeled 18-nucleotide DNA primer (Table 1). As shown in Fig. 1*B*, EFdA-TP suppressed full-length DNA synthesis by RT in a dose-dependent manner. EFdA-TP was between ~1 and 2 orders of magnitude more effective at inhibiting RT-catalyzed DNA synthesis than any of the NRTIs evaluated. The IC_{50} for suppression of full primer extension by EFdA-TP was 14 nM using the longer T_{d100}/P_{d18} (Fig. 1, *C* and *D*). To confirm the high efficiency at which RT uses EFdA, we performed single nucleotide incorporation assays under steady state conditions (using T_{d31}/P_{d18} or T_{r31}/P_{d18} as a T/P, Table 1). Our results show that under these conditions the incorporation efficiency (k_{cat}/K_m) of EFdA-TP by RT is twice that for the natural dATP substrate and four times that for ddATP, primarily because of changes in the K_m of RT to these substrates (Table 3). Moreover, we found that the increase in incorporation efficiency of EFdA-TP could be even higher at different nucleic acid sub-

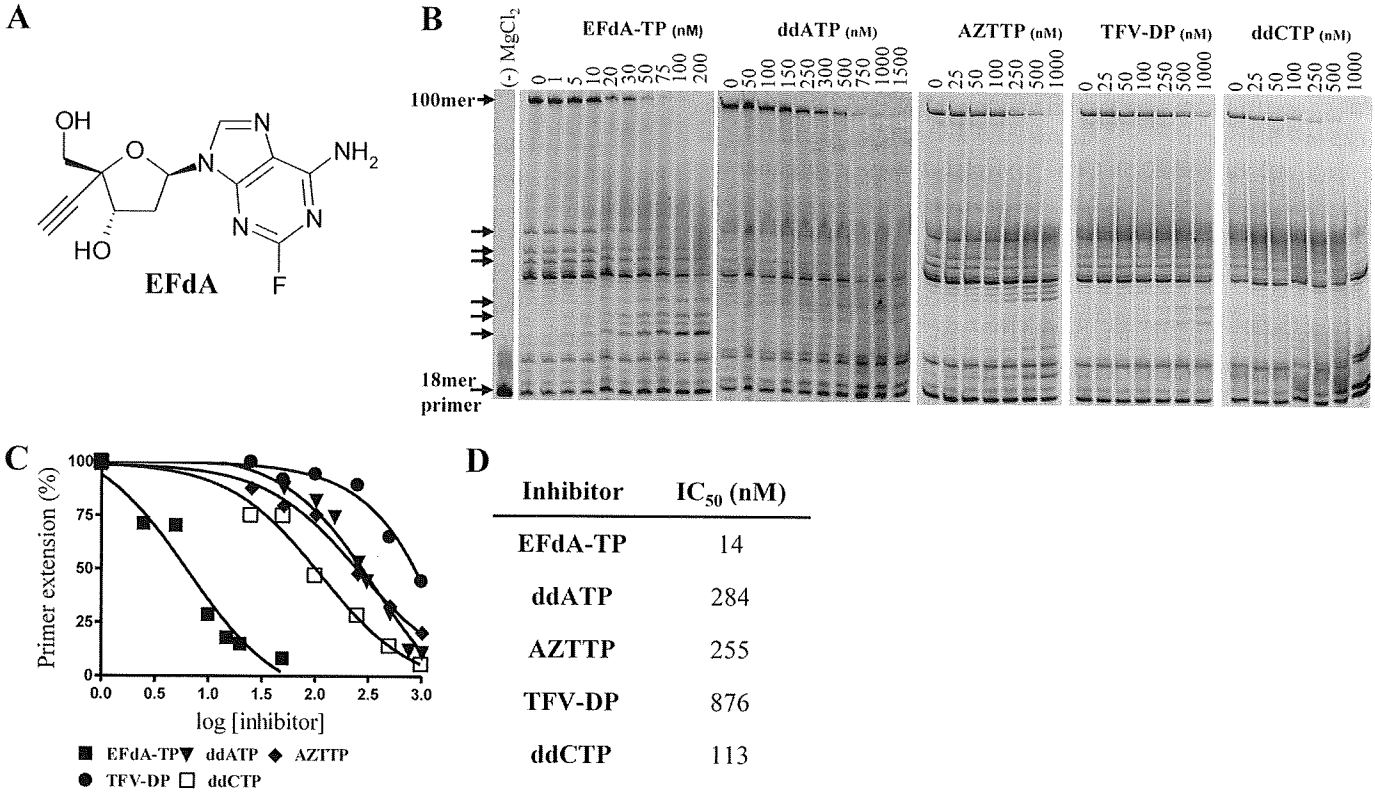

FIGURE 1. **HIV RT inhibition by EFdA-TP and other NRTIs.** *A*, structure of EFdA. *B*, primer extension by HIV-1 RT was observed in the presence of fixed concentrations of 4 dNTPs, T_{d100}/P_{d18}, and $MgCl_2$ and increasing concentrations of EFdA-TP, ddATP, AZTTP, TFV-DP, or ddCTP. The reactions were carried out for 15 min. The *arrows* denote stops of the elongating DNA chain where adenosine analogs (EFdA-TP, ddATP, or TFV-DP) were expected to be incorporated. The *first lane* is a negative control, where no $MgCl_2$ was added; it shows the length of the 18-mer primer. *C*, the 100-mer products synthesized by HIV-1 RT were quantified and plotted against increasing concentrations of various inhibitors. The data points were fitted by GraphPad Prism 4. *D*, IC_{50} values of the nucleotide analogs were determined by quantifying the percent of full extension and fitting the data points to GraphPad Prism 4 using one-site competition nonlinear regression.

TABLE 3

Steady state kinetic parameters (K_m and k_{cat}) for EFdA-MP and dAMP incorporation by HIV-1 RT

Values are means ± S.D. of triplicate determinations and were determined from Michaelis-Menten equation using GraphPad Prism 4. ND, not determined.

dNTP	T/P (DNA/DNA)				T/P (RNA/DNA)			
	K_m	k_{cat}	k_{cat}/K_m	Selectivity[a]	K_m	k_{cat}	k_{cat}/K_m	Selectivity[a]
	nM	min^{-1}	$min^{-1} \cdot nM^{-1}$		*nM*	min^{-1}	$min^{-1} \cdot nM^{-1}$	
dATP	73.11 ± 11	19.9 ± 0.7	0.272	1	21.3 ± 8	3.1 ± 0.2	0.145	1
EFdA-TP	39.2 ± 3	21.1 ± 0.4	0.538	2	24.1 ± 5	2.3 ± 0.1	0.095	0.7
ddATP	97.0 ± 9	15.4 ± 0.3	0.159	0.6	ND	ND	ND	ND

[a] Selectivity is the ratio of the incorporation efficiency (k_{cat}/K_m) of EFdA-MP or ddAMP over that of dAMP ($[k_{cat}/K_m]_{EFdA\text{-}MP}/[k_{cat}/K_m]_{dAMP}$ or $[k_{cat}/K_m]_{ddAMP}/[k_{cat}/K_m]_{dAMP}$).

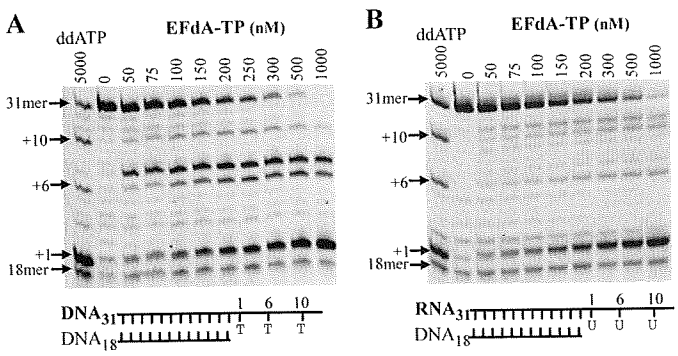

FIGURE 2. **Inhibition of DNA- and RNA-dependent DNA synthesis by EFdA-TP.** *A*, T_{d31}/P_{d18} was incubated with HIV-1 RT for 15 min in the presence of 1 μM dNTPs and $MgCl_2$ and increasing concentrations of EFdA-TP (0–1000 nM). The *first lane* (dd*ATP*) shows the inhibition of primer extension by ddATP to identify points of adenosine analog (ddATP or EFdA-TP) incorporation (*arrows*: +1, +6, and +10). *B*, the primer extension under the same conditions with an RNA/DNA substrate containing an RNA template annealed to a DNA primer (T_{r31}/P_{d18}).

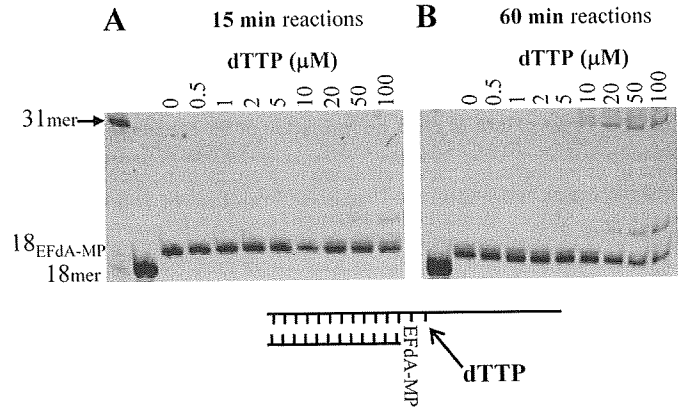

FIGURE 3. **Incorporation of dNTP on EFdA-terminated template/primer ($T/P_{EFdA\text{-}MP}$).** EFdA-TP was first incorporated at T_{d31}/P_{d18} by HIV-1 RT and purified as described under "Experimental Procedures." The incorporation of the next incoming nucleotide on $T/P_{EFdA\text{-}MP}$ was examined in the presence of HIV-1 RT and $MgCl_2$ and increasing concentrations of dTTP. All other dNTPs were at a concentration of 1 μM. The reactions were stopped after 15 min (*A*) and 60 min (*B*).

strate sequences, more than 10 times higher than dATP (data not shown).

The EFdA-TP-mediated reduction in full-length DNA synthesis was accompanied by the concomitant appearance of products corresponding to the primer extension only at the length expected for the incorporation of adenosine nucleotides (indicated by *arrows* in Fig. 1*B*). Neither ddATP nor TFV-DP provided significant accumulation of this small DNA product.

EFdA-TP Inhibits DNA Synthesis Mainly at the Point of Incorporation—The stopping patterns of DNA synthesis were different in the presence of EFdA-TP compared with other dATP analogs such as ddATP and TFV-DP (marked by *arrows* in Fig. 1*B*). Hence, we used a shorter template (T_{d31}/P_{d18} (Table 1)), which allowed unambiguous identification of the stopping sites. As expected, the inhibitory potential of EFdA (and other NRTIs) appears lower in these shorter T/P (IC_{50} for suppression of full primer extension was 104 nM) in which there are fewer opportunities for incorporation (24). This substrate allows incorporation of dA, ddA, or EFdA at positions 1, 6, and 10 (Fig. 2). The results show that EFdA-TP causes major pauses at all possible points of incorporation ((Fig. 2*A*, positions 1, 6, and 10), suggesting that EFdA-TP inhibits RT mainly as an obligate chain terminator. Notably, there was a distinct difference at position +6 of T_{d31}/P_{d18}, where we observed a strong stop not only at the point of incorporation but also at the position following (Fig. 2*A*, positions 6 and 7, respectively). These results suggest that in some cases EFdA-MP may also allow incorporation of an additional nucleotide depending upon the template sequence.

EFdA-TP inhibits both RNA- and DNA-dependent RT-catalyzed full-length DNA polymerization to comparable extents (Fig. 2). The selectivity for incorporation of EFdA-MP over dAMP ($(k_{cat}/K_m)_{EFdA\text{-}TP}/(k_{cat}/K_m)_{dATP}$) was slightly increased when we used DNA/DNA *versus* RNA/DNA template/primers (Table 3, 2 *versus* 0.7). Notably, the overall pausing pattern due to inhibition by EFdA-TP differs depending on whether the template is RNA or DNA. Inhibition differences based on type and sequence of template are currently under investigation.

Extension of EFdA-terminated T/P ($T/P_{EFdA\text{-}MP}$)—The data in Figs. 1 and 2 suggest that EFdA-TP can act as a terminator of RT-catalyzed DNA synthesis in a manner similar to that of other NRTI-TPs. We therefore examined the efficiency of nucleotide additions to primers that were synthesized to already possess a 3′-terminal EFdA-MP. Fig. 3 shows that the primer extension from EFdA-MP is very limited and is evident only at very high and nonphysiological concentrations (>50 μM) of the next nucleotide and with extended reaction times (Fig. 3*B*, 60-min incubation). It therefore appears that EFdA acts as a *de facto* chain terminator, despite the presence of a 3′-OH function.

RT Binds T/P_{ddAMP} and $T/P_{EFdA\text{-}MP}$ at Similar Efficiencies—A possible reason for the inability of RT to efficiently extend the EFdA-MP-terminated primer is that it binds $T/P_{EFdA\text{-}MP}$ with less affinity than it does a T/P lacking a 3′-terminal EFdA-MP nucleotide. We therefore used gel mobility shift assays to compare the stabilities of the binary complexes of RT with T/P possessing either EFdA-MP ($T/P_{EFdA\text{-}MP}$) or ddAMP

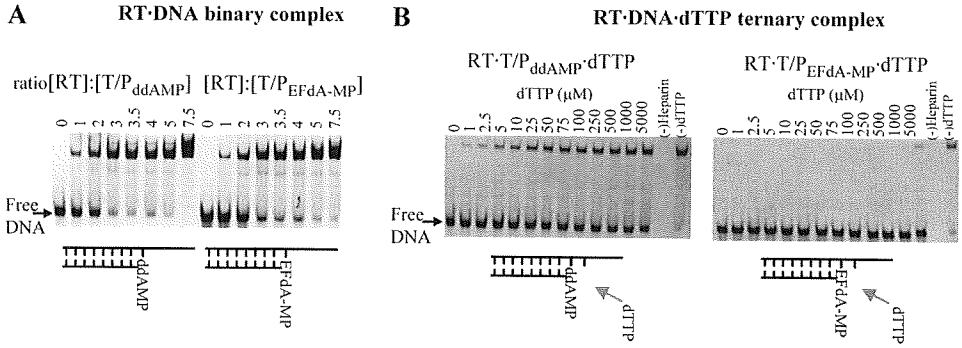

FIGURE 4. **Effect of ddA or EFdA on formation of binary and ternary complexes.** *A*, formation of a binary complex between RT and T/P_{ddAMP} or $T/P_{EFdA\text{-}MP}$. Purified T/P_{ddAMP} or $T/P_{EFdA\text{-}MP}$ (20 nM) was incubated with HIV-1 RT at the indicated molar ratios and resolved by nondenaturing gel electrophoresis. *B*, formation of a ternary complex between RT and T/P_{ddAMP} or $T/P_{EFdA\text{-}MP}$ and incoming dTTP. The stability of the ternary complexes was analyzed by incubating 100 nM RT and 9 nM T/P_{ddAMP} or $T/P_{EFdA\text{-}MP}$ in the presence of increasing dTTP concentrations and heparin, which acted as an enzyme trap. In the absence of dTTP, the T/P·RT binary complex is unstable (*lane 0*), as RT dissociates from the T/P and is trapped by heparin.

(T/P_{ddAMP}) at the 3′-primer terminus (T/P chain terminated by EFdA-MP or ddAMP). As shown in Fig. 4*A*, RT binds $T/P_{EFdA\text{-}MP}$ with an apparent affinity comparable with that of the normal T/P (K_d for RT·$T/P_{EFdA\text{-}MP}$ = 51 nM; K_d for RT·$T/P_{ddA\text{-}MP}$ = 42 nM). This observation suggests that RT is inhibited at a downstream step in the polymerization reaction.

RT Is Unable to Form a Stable Ternary Complex with $T/P_{EFdA\text{-}MP}$ and dNTP—The next step in the DNA polymerization mechanism is the binding of the next complementary dNTP to RT·DNA, thus forming the ternary complex that precedes catalysis. To determine whether EFdA exerts its inhibitory effect by interfering with the formation of a stable ternary complex with the incoming dNTP, we used a gel-based nondenaturing electrophoresis assay (25) that detects the ternary complex formed by RT·T/P and the next complementary dNTP (in this case, dTTP). In this assay, the stability of the ternary complex is assessed by the persistence of the RT·DNA·dNTP complex upon addition of a competing heparin trap (25). As seen in Fig. 4*B* (*left panel*), the ternary complex formed by RT with T/P_{ddAMP} and dTTP is quite stable. In contrast, no significant amount of ternary complex was noted in assays using $T/P_{EFdA\text{-}MP}$ even at very high dTTP concentrations (Fig. 4*B*, *right panel*).

Incorporation of EFdA-TP into DNA ($T/P_{EFdA\text{-}MP}$) Decreases Translocation of RT—The inability of RT to form a stable ternary complex with $T/P_{EFdA\text{-}MP}$ and the next complementary dNTP could arise from several factors including (i) the inability of the 3′-terminal EFdA-MP primer to efficiently translocate from the N-site (which is also the pre-translocation site) to the post-translocation primer site (P-site), thereby preventing the next incoming nucleotide from binding; and (ii) the fact that $T/P_{EFdA\text{-}MP}$ *can* translocate, but the presence of unnatural substituents in the primer 3′-terminal EFdA-MP (4′-ethynyl and 2-fluoro) may alter geometric and electronic parameters at the primer end, thus preventing efficient incorporation of the next incoming dNTP such that catalysis cannot occur. These two different possibilities place the nucleic acid at different positions/registers with respect to a site-specific landmark in RT, the metal-binding ribonuclease H (RNase H) active site, as shown in the schematic of Fig. 5*B*. We therefore used a site-specific Fe^{2+} footprinting assay (19) to determine whether the primer 3′-terminal EFdA-MP of the RT·$T/P_{EFdA\text{-}MP}$ complex resides primarily in the pre- (N-site) or post-translocation (P-site) state in the absence and the presence of varying levels of the incoming complementary dNTP, which serves to "force" the 3′-primer terminus from the pre-translocation (N-site) to the post-translocation site (P-site). As shown on Fig. 5*A* (*left panel*), in the absence of dTTP (*first lane*), primers with a 3′-terminal ddAMP are located in both the pre- and post-translocation sites in approximately equal amounts, and the addition of the next complementary nucleotide (dTTP) forces the primer 3′-end almost entirely into the post-translocation site. In contrast, in the absence of dTTP, primers with a 3′-terminal EFdA-MP are located exclusively in the pre-translocation site (Fig. 5*A*, *right panel*, *first lane*). The next complementary nucleotide (dTTP) is unable to shift the position of the 3′-EFdA-MP except at very high (nonphysiological) concentrations.

Because it is physically impossible for the incoming dNTP to bind at the N-site (dNTP-binding site) when it is occupied by the 3′-primer terminus of the non-translocated $T/P_{EFdA\text{-}MP}$, the present data demonstrate that the apparent termination of RT-catalyzed DNA synthesis upon incorporation of EFdA-MP arises from the inability of the 3′-EFdA-MP-terminated primer/template ($T/P_{EFdA\text{-}MP}$) to efficiently translocate to the P-site and allow incorporation of the next dNTP. Moreover, the latter is unable to force translocation of the 3′-EFdA-MP-terminated primer strand. The inability of the 3′-EFdA-MP-terminated primer to translocate to allow binding of the next complementary dNTP effectively prevents continued elongation of the nascent viral DNA, despite the presence of the 3′-OH on EFdA. Therefore, we propose that EFdA acts as a *translocation-defective reverse transcriptase inhibitor.*

Phosphorolytic Excision of EFdA-MP—Two major mechanisms account for HIV resistance to NRTIs (26). One is based on NRTI discrimination, where the mutant RT preferentially incorporates the natural dNTP rather than the NRTI-TP. The other major resistance mechanism involves ATP-mediated phosphorolytic excision of the incorporated chain-terminating NRTI from the 3′-end of the primer (27, 28). We and others have previously shown that for excision to occur, the 3′-end of the primer must be positioned at the pre-translocation or N-site of RT (19, 29, 30). As we have already shown, the 3′-EFdA-MP-terminated primer strand binds predominantly in a pre-translocation mode. This suggests that EFdA-terminated primers might be especially susceptible to RT-catalyzed phosphorolytic removal of the terminating EFdA-MP. To assess this possibility we carried out primer unblocking experiments using nucleic acid substrates having at the 3′-primer terminus either EFdA-MP or ddAMP ($T/P_{EFdA\text{-}MP}$ or T/P_{ddAMP}, respectively). The quantitation of results in Fig. 6*A*

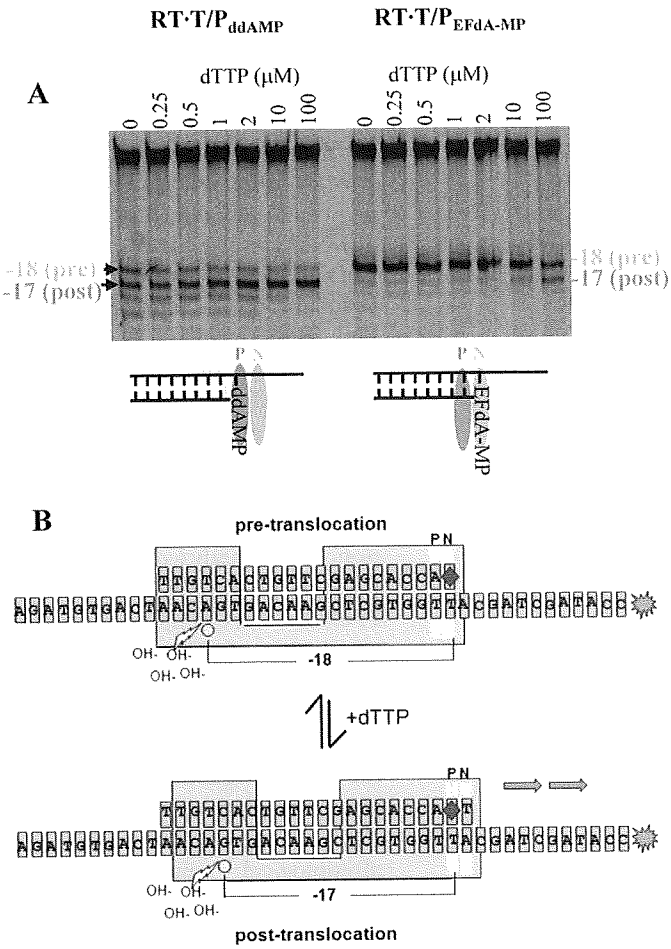

FIGURE 5. **Determination of the translocation state of RT bound to T/P$_{ddAMP}$ and T/P$_{EFdA-MP}$ template/primers.** *A*, the translocation state of RT after EFdA-MP incorporation was determined using site-specific Fe^{2+} footprinting. T/P$_{ddAMP}$ or T/P$_{EFdA-MP}$ (100 nM) with 5′-Cy3 label on the DNA template (see Fig. 5*B*) was incubated with HIV-1 RT (600 nM) and various concentrations of the next incoming nucleotide (dTTP) (as indicated). The complexes were treated for 5 min with ammonium iron sulfate (1 mM) and resolved on a polyacrylamide 7 M urea gel. An excision at position −18 indicates a pre-translocation complex, whereas the excision at position −17 represents a post-translocation complex. The scheme below the gel images indicates that in the absence of incoming dNTP, T/P$_{ddAMP}$ is bound mostly in a post-translocation state, whereas T/P$_{EFdA-MP}$ is bound in a pre-translocation state, with EFdA-MP positioned at the N-site. *B*, schematic of the excision assay. Depending on whether the 3′-primer terminus is positioned at the pre-translocation (N-site) or post-translocation (P-site) site, cleavage is observed on the 5′-labeled template strand at positions −18 or −17, respectively. The addition of varying levels of the incoming complementary dNTP serves to force the 3′-primer terminus from the N-site to the P-site.

shows that the rate of hydrolysis of ddAMP- and EFdA-MP-terminated primers was 0.5 and 1.6 min^{-1}, respectively. We also considered whether the EFdA-TP formed upon pyrophosphorolytic removal of the 3′-terminal EFdA-MP was promptly reincorporated. We tested this possibility using so-called phosphorolysis "rescue" assays, where in addition to the PP_i that would react with the EFdA-MP from the 3′-primer terminus to produce EFdA-TP, we also included a high concentration of dATP that would compete with and prevent reincorporation of EFdA-TP. In the case of high excision activity, we expected to see higher bands corresponding to rescued and extended primers. Indeed, substantially more primer extension was noted in PP_i- or ATP-mediated rescue assays using 3′-terminal EFdA-MP primers (Fig. 6, *C* and *D*, *right panels*) than in assays using primers with 3′-terminal ddAMP (Fig. 6, *C* and *D*, *left panels*). The rate for the ATP-dependent rescue of EFdA-MP-terminated primer was 0.063 min^{-1}. The corresponding rate for the ATP-dependent rescue of the ddAMP-terminated primer could not be calculated because the reaction was very slow. Collectively, these data suggest that 3′-terminal EFdA-MP is phosphorolytically excised more efficiently than ddAMP, consistent with its preferential positioning at the phosphorolysis-susceptible pre-translocation N-site.

Molecular Basis of RT Inhibition by TDRTIs—To understand the molecular basis of RT inhibition by EFdA-TP, we built molecular models of complexes that represent the following intermediates of the DNA polymerization reaction: 1) a pre-catalytic RT·DNA·EFdA-TP ternary complex and 2) a complex that corresponds to the product of EFdA-MP incorporation *prior* to translocation. Previously we had solved crystal structures representing both types of these intermediates for other NRTIs (29, 31), and the model building was guided by the structural characteristics of these complexes. Moreover, we built the EFdA sugar ring in both models in a 3′-endo (North) conformation based on our unpublished NMR experimental data, which clearly show that the equilibrium of the geometries of the EFdA sugar ring overwhelmingly favors the 3′-endo conformation (North). The RT·DNA·EFdA-TP ternary complex model was built using as a starting structure the coordinates of our RT·DNA·TFV-DP crystal structure (PDB code 1T05), not only because it is the highest resolution structure of an RT ternary complex but also because it is the only structure of RT in complex with an analog of deoxyadenosine triphosphate (31). The model of the RT·DNA·EFdA-TP complex represents the step of EFdA-TP binding to the preformed RT·DNA complex (Fig. 7*A*). It had no significant differences from the crystal structures of the ternary complexes of RT with DNA and TFV-DP (PDB code 1T05) or dTTP (PDB code 1RTD). It shows that the 4′-ethynyl of EFdA-TP is favorably positioned in a hydrophobic pocket formed by Ala-114, Tyr-115, Phe-160, and Met-184 and the aliphatic portion of Asp-185. These interactions are similar to those that have been proposed for binding of 4′-Ed4T, a related NRTI thymidine analog that also has a 4′-substitution but no 3′-OH group (32). These interactions are also consistent with the observed high efficiency of EFdA-MP incorporation by RT (Fig. 1*D*). Similar interactions stabilize the RT·DNA$_{EFdA-MP}$ pre-translocation binary complex, which has the primer 3′-terminal EFdA-MP positioned at the N-site (Fig. 7*B*, pre-translocation complex). These favorable interactions are also consistent with the enhanced binding of T/P$_{EFdA-MP}$ in a pre-translocated mode (Fig. 5).

DISCUSSION

The single most distinguishing feature of NRTIs used in HIV therapy is the absence of a 3′-OH. This property results in termination of further viral DNA synthesis upon incorporation of the inhibitor into the nascent viral DNA. We have shown (10, 13) that certain nucleoside analogs that retain the 3′-OH group can exert potent antiviral activity. One of these, EFdA, inhibits HIV-1 replication in PBMCs with a potency that is several orders of magnitude greater than that of any of the current

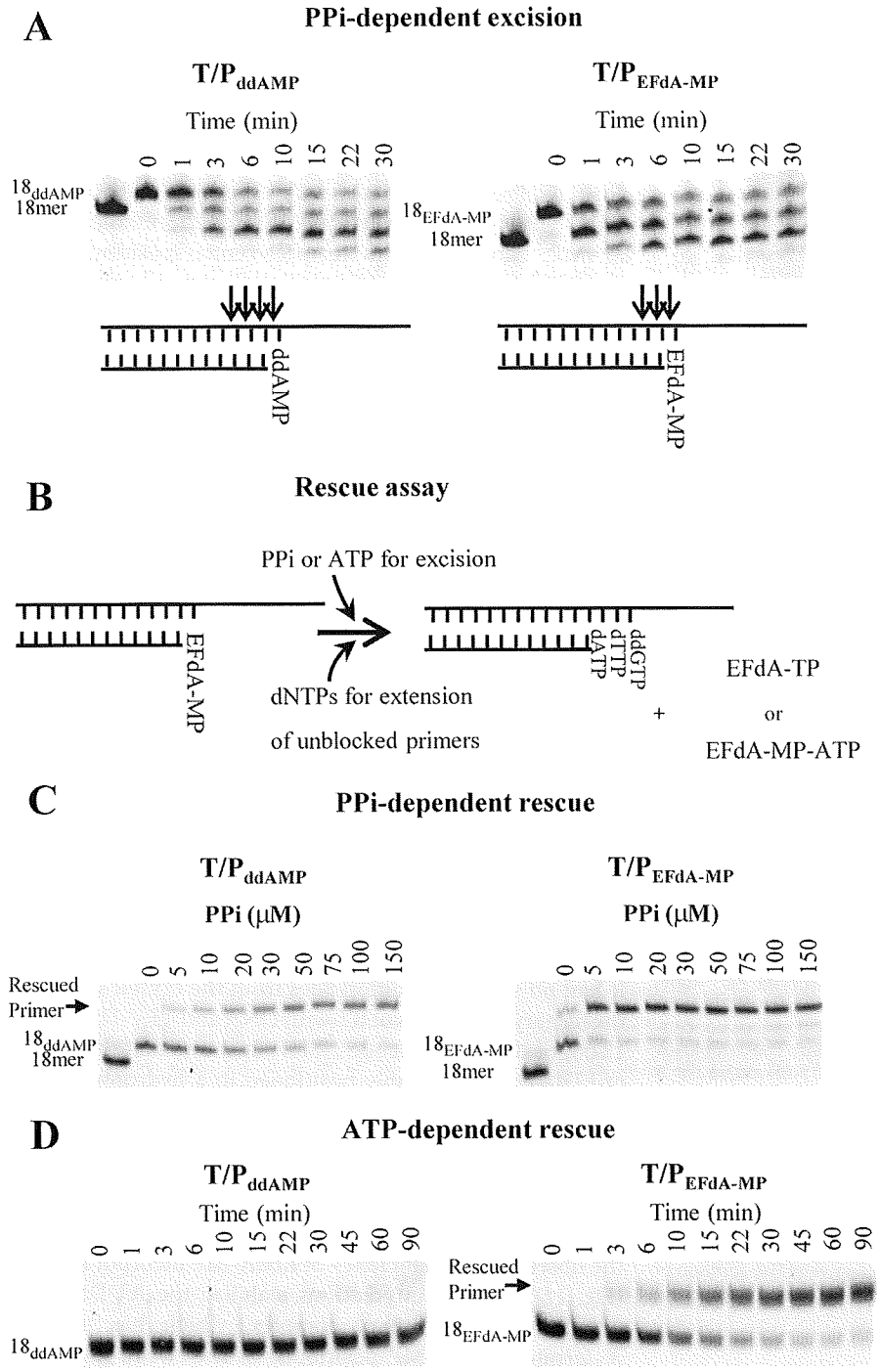

FIGURE 6. **PP_i and ATP-dependent unblocking of ddAMP and EFdA-MP terminated primers.** *A*, PP_i-dependent unblocking of T/P_{ddAMP} and $T/P_{EFdA\text{-}MP}$. Purified T/P_{ddAMP} or $T/P_{EFdA\text{-}MP}$ was incubated with HIV-1 RT in the presence of 6 mM $MgCl_2$ and 150 μM PP_i at 37 °C. Aliquots were removed and reactions stopped at the indicated time points (0–30 min). Cleavage sites are indicated with *arrows* in the schemes below the gels. *B*, schematic representation of PP_i- and ATP-dependent rescue assay. The excision products of PP_i- and ATP-dependent excision of EFdA-MP are EFdA-TP and the EFdA-MP-ATP dinucleoside tetraphosphate, respectively. *C*, PP_i-dependent rescue of T/P_{ddAMP} and $T/P_{EFdA\text{-}MP}$. Purified $T/P_{EFdA\text{-}MP}$ or T/P_{ddAMP} was incubated with HIV-1 RT in the presence of various amounts of PP_i (0–150 μM), dATP (100 μM), dTTP (0.5 μM), or ddGTP (10 μM) and 10 mM $MgCl_2$ at 37 °C. Aliquots of the reaction were stopped after 10 min. *D*, ATP-dependent rescue of T/P_{ddAMP} or $T/P_{EFdA\text{-}MP}$. Purified $T/P_{EFdA\text{-}MP}$ or T/P_{ddAMP} was incubated with HIV-1 RT in the presence of ATP (3.5 mM), dATP (100 μM), dTTP (0.5 μM), or ddGTP (10 μM) and 10 mM $MgCl_2$ at 37 °C. Aliquots of the reaction were stopped at the indicated time points (0–90 min).

clinically used NRTIs (Table 2 and Ref. 23), consistent with the inhibitory data obtained in transformed T-cell lines (13). The molecular basis for this exceptional antiviral activity of EFdA has to date been unclear. The detailed *in vitro* biochemical studies presented in this article show that EFdA inhibits HIV-1 reverse transcriptase mainly by blocking translocation after incorporation at the 3′-primer end and functioning as a TDRTI. The specificity of inhibition can vary depending on the type and sequence of the template (Fig. 2). Our studies also suggest that both the 3′-OH and the 4′-ethynyl groups of EFdA play important roles in the high antiviral potency exerted by this nucleoside analog.

The 4′-ethynyl group is essential for the mechanism of EFdA inhibition of RT-catalyzed DNA synthesis. The present work shows that EFdA-TP acts mainly as a potent terminator of RT-catalyzed DNA synthesis, despite having a 3′-OH group. It is possible that the presence of a 4′-ethynyl substitution on the ribose ring somehow affects the geometry and reactivity of its 3′-OH. However, in the presence of physiological concentrations of dNTPs (<50 μM) the chain terminating activity of EFdA appears to arise mainly from the difficulty of RT to translocate the 3′-EFdA-MP-terminated primer ($T/P_{EFdA\text{-}MP}$) following incorporation of the inhibitor. Under these circumstances the dNTP-binding site is not accessible, and incorporation of the next complementary nucleotide is prevented (Fig. 7*C*). Hence, EFdA appears to act as a translocation-defective RT inhibitor. The 4′-ethynyl moiety appears to be the critical factor in the difficulty presented by translocation of DNA primers with a 3′-terminal EFdA-MP residue. Our molecular model of the RT·DNA·EFdA-TP ternary complex suggests that the 4′-ethynyl moiety fits nicely into a hydrophobic pocket in the RT active site defined by residues Ala-114, Tyr-115, Phe-160, and Met-184 and the aliphatic portion of Asp-185 (Fig. 7*A*), similar to the proposed interactions of 4′-Ed4T at the same site (32). Once EFdA-MP has been added to the primer end to form the pre-translocation (or N-site) reaction product, these same RT residues serve to stabilize the terminal EFdA-MP in

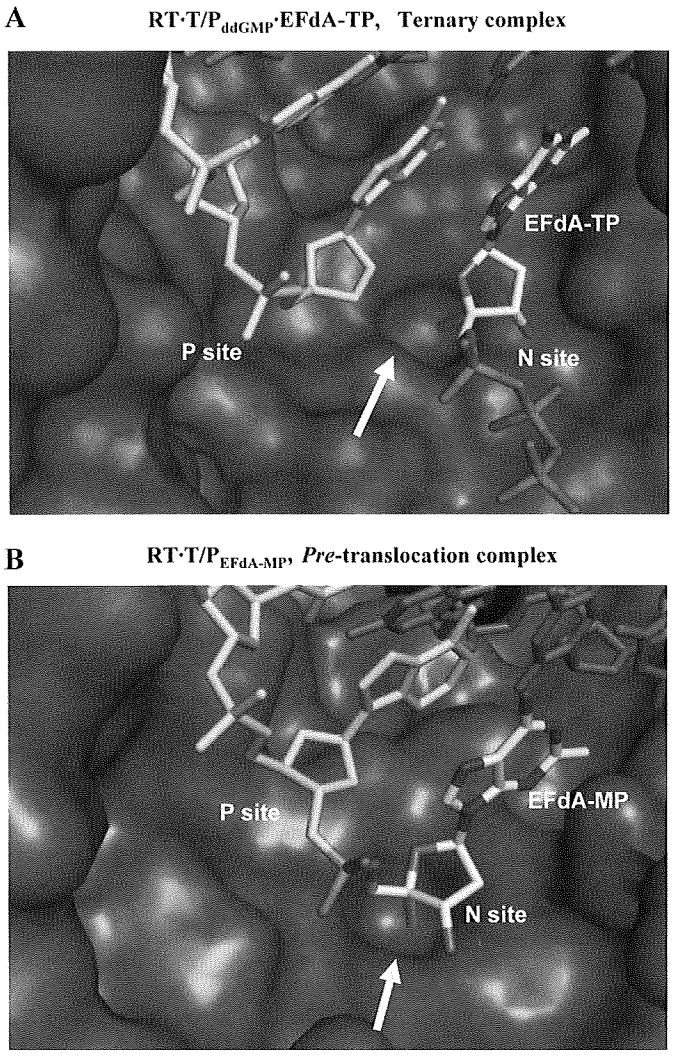

FIGURE 7. **Molecular models representing intermediates of the DNA polymerization reaction.** *A*, molecular model of a ternary complex among RT, DNA, and EFdA-TP. The primer is bound at the P-site, and the incoming EFdA-TP is bound at the N-site. The 4′-ethynyl group of EFdA-TP is bound at a hydrophobic pocket (shown by a *yellow arrow*) defined by residues Met-184, Ala-114, Tyr-115, and Phe-160 and the aliphatic chain of Asp-185. For purposes of clarity the p66 fingers subdomain is not shown. *B*, molecular model of RT bound to EFdA-MP-terminated T/P immediately after incorporation of the inhibitor at the primer terminus and before translocation. The EFdA-MP of the 3′-primer terminus is positioned at the N-site. *C*, schematic representation of RT inhibition by EFdA. After incorporation of EFdA-MP at the 3′-primer terminus RT remains bound to T/P$_{EFdA}$ mostly in a pre-translocation binding mode (*top*). In that binding mode the EFdA-MP at the 3′-primer terminus blocks binding of the incoming dNTP, thus inhibiting DNA polymerization.

the pre-translocation state (Fig. 7*B*). Hence, the stabilization of the primer 3′-terminal EFdA-MP in the pre-translocation state helps it to remain in a position antagonistic to further nucleotide addition and to inhibit DNA polymerization (Fig. 7*C*).

We have observed that in one instance RT stopped not only at the point of EFdA incorporation but also at the position following (Fig. 2*A*, positions *6* and *7*, respectively). Interestingly, we found that RT has enhanced translocation efficiency at this site, both on T/P$_{EFdA-MP}$ and on T/P$_{ddAMP}$ (data not shown). It appears that some translocated T/P$_{EFdA-MP}$ is also elongated by an additional nucleotide. Further polymerization may be inhibited by unfavorable interactions between the 4′-ethynyl group in the elongated template/primer (T/P$_{EFdA-MP-dNMP}$) with protein residues upstream in the DNA-binding cleft. The effect of template on the inhibition mechanism by EFdA is the subject of an ongoing investigation.

RT-catalyzed phosphorolytic excision of chain-terminating NRTIs is a major mechanism of HIV-1 resistance to the nucleoside analog class of therapeutics (26–28, 33). Our previous studies have shown that the NRTI phosphorolytic excision reaction is favored when the primer 3′-terminal nucleotide is in the pre-translocation or N-site (19, 34). The preference of the primer 3′-terminal EFdA-MP to remain in this site suggests that terminal EFdA-MP should undergo facile phosphorolytic removal. EFdA-MP was subject to excision by pyrophosphorolysis somehow faster than ddAMP, which tends to localize in the post-translocation site when at the 3′ terminus of the primer (see Fig. 5*A*). Although EFdA-MP can undergo excision, this process is not overly efficient, apparently because once the nucleotide is excised through pyrophosphorolysis to form EFdA-TP, the latter is rapidly reincorporated. These findings suggest that phosphorolysis may not play a significant role in HIV-1 resistance to EFdA, consistent with the relatively small loss of antiviral potency of EFdA against excision-enhanced HIV-1-containing mutations associated with resistance to AZT (13).

The importance of the 3′-OH in antiviral activity of EFdA is perhaps best highlighted by the observation that EFdA is 10,000-fold more potent at inhibiting HIV-1 replication in PBMCs than is the identical nucleoside lacking a 3′-OH, namely EFddA (Table 2). The 3′-OH on EFdA appears to play a number of roles in contributing to the exceptional antiviral potency of the compound. The 3′-OH on natural dNTP substrates contributes to the efficiency with which RT uses these substrates, and in general NRTIs that lack a 3′-OH are used less efficiently by RT than the base-analogous dNTP (35) (Table 3). Our *in vitro* biochemical data demonstrate that EFdA-TP is approximately 1 and 2 orders of magnitude more potent an inhibitor of RT-catalyzed DNA synthesis *in vitro* than are the

adenine-based NRTIs ddATP and TFV-DP, respectively (Fig. 1*D*), neither of which has a 3′-OH. Indeed, it appears that under identical conditions, RT is at least twice as likely to use EFdA-TP as a substrate over the natural nucleotide dATP (Table 3). This suggests that during HIV-1 reverse transcription, EFdA-TP might be preferentially incorporated, thereby leading to early and profound chain termination and contributing to the observed potent antiviral activity of this nucleoside analog.

NRTIs are administered therapeutically as prodrugs; these must undergo phosphorylation in target cells in order to exert their antiviral activity. The lack of a 3′-OH on current clinically used NRTIs can reduce recognition by cellular nucleoside/nucleotide kinases that have evolved to interact with the 3′-OH present in their natural nucleoside substrates (9). Preliminary studies suggest that EFdA appears to undergo rapid and facile intracellular conversion to the active antiviral EFdA-TP (36), showing that the 4′-ethynyl group does not interfere with recognition by cellular nucleoside/nucleotide kinases. Furthermore, the presence of fluorine at position 2 of the adenine base of EFdA helps to stabilize intracellular levels of EFdA and its phosphorylated products by hindering adenosine deaminase-catalyzed degradation of the molecule (13). Thus, both the 2-fluoro and the 3′-OH of EFdA may contribute to the intracellular accumulation of the antiviral EFdA-TP, thereby leading to its pronounced antiviral activity. We are presently carrying out detailed studies of the intracellular pharmacokinetics of EFdA in comparison with other NRTIs to better understand the dynamics of EFdA phosphorylation and turnover as contributors to the exceptional potency and persistence of its antiviral activity.

Other nucleoside analog inhibitors of HIV-1 RT that possess a 3′-OH have been described (21, 37–42), although these have mechanisms of action quite distinct from that of EFdA. North-methanocarba-2′-deoxyadenosine triphosphate and North-methanocarba-2′-thymidine triphosphate inhibit HIV-1 RT *in vitro* by a mechanism of delayed chain termination, where RT-catalyzed DNA synthesis pauses after the addition of several nucleotides following incorporation of the inhibitor (38, 39). Neither of these compounds has antiviral activity, presumably because of poor intracellular phosphorylation. Entecavir is a nucleoside analog with a 3′-OH that is approved for treatment of hepatitis B infection. Entecavir-TP also has been shown to inhibit HIV-1 RT-catalyzed DNA synthesis by a mechanism of delayed chain termination (40). Entecavir has only weak antiviral activity against HIV-1.

Additionally, nucleoside analogs substituted at the 4′-position have also been described previously (43–46). For example, 4′-azidothymidine and 4′-azidoadenosine both inhibit HIV-1 replication (46) although with potencies 200–2000-fold less than that of EFdA. Both 4′-azido nucleosides also have poor *in vitro* selectivity indices because of significant cytotoxicity. Azidothymidine-TP was shown to inhibit RT-catalyzed DNA synthesis by a type of delayed chain termination; incorporation of two sequential azidothymidine-MP molecules blocked DNA synthesis (44, 45). 4′-Methyl thymidine and 4′-ethyl thymidine both seem to cause pauses and stops in DNA synthesis at the point of incorporation (39). However, neither of these compounds has antiviral activity, because they cannot be phosphorylated by cellular nucleoside kinases. An analog of d4T that has a 4′-ethynyl substitution (Ed4T) is ~10 times more active than the parent compound (47, 48). Because Ed4T lacks a 3′-OH, it inhibits RT as a conventional chain terminator. Interestingly, Ed4T is a better substrate than d4T for phosphorylation by human thymidine kinase 1 (47–50), a property that leads to its increased antiviral potency compared with d4T. The antiviral activity of Ed4T is ~50-fold lower than that of EFdA.

In summary, EFdA is a TDRTI with two functionalities lacking in current therapeutic NRTIs, namely a 4′-ethynyl group and a 3′-OH. These additional properties impart superior antiviral activity to the compound and contribute to its mechanism of action, namely inhibition of primer translocation following EFdA-MP incorporation. This mechanism allows EFdA to act mainly as a *de facto* chain terminator of RT-catalyzed DNA synthesis, despite the presence of a 3′-OH. The present study validates RT nucleic acid translocation as a potential therapeutic target.

REFERENCES

1. Hammer, S. M., Saag, M. S., Schechter, M., Montaner, J. S., Schooley, R. T., Jacobsen, D. M., Thompson, M. A., Carpenter, C. C., Fischl, M. A., Gazzard, B. G., Gatell, J. M., Hirsch, M. S., Katzenstein, D. A., Richman, D. D., Vella, S., Yeni, P. G., and Volberding, P. A. (2006) *Top. HIV Med.* **14,** 827–843
2. Schinazi, R. F., Hernandez-Santiago, B. I., and Hurwitz, S. J. (2006) *Antiviral Res.* **71,** 322–334
3. Parniak, M. A., and Sluis-Cremer, N. (2000) *Adv. Pharmacol.* **49,** 67–109
4. De Clercq, E. (2007) *Verh. K. Acad. Geneeskd. Belg.* **69,** 81–104
5. Sluis-Cremer, N., and Tachedjian, G. (2008) *Virus Res.* **134,** 147–156
6. Deval, J. (2009) *Drugs* **69,** 151–166
7. Sharma, P. L., Nurpeisov, V., Hernandez-Santiago, B., Beltran, T., and Schinazi, R. F. (2004) *Curr. Top. Med. Chem.* **4,** 895–919
8. Sarafianos, S. G., Marchand, B., Das, K., Himmel, D. M., Parniak, M. A., Hughes, S. H., and Arnold, E. (2009) *J. Mol. Biol.* **385,** 693–713
9. Gallois-Montbrun, S., Schneider, B., Chen, Y., Giacomoni-Fernandes, V., Mulard, L., Morera, S., Janin, J., Deville-Bonne, D., and Veron, M. (2002) *J. Biol. Chem.* **277,** 39953–39959
10. Kodama, E. I., Kohgo, S., Kitano, K., Machida, H., Gatanaga, H., Shigeta, S., Matsuoka, M., Ohrui, H., and Mitsuya, H. (2001) *Antimicrob. Agents Chemother.* **45,** 1539–1546
11. Ohrui, H., and Mitsuya, H. (2001) *Curr. Drug Targets Infect. Disord.* **1,** 1–10
12. Ohrui, H., Kohgo, S., Hayakawa, H., Kodama, E., Matsuoka, M., Nakata, T., and Mitsuya, H. (2006) *Nucleic Acids Symp. Ser. (Oxf.) 2006,* 1–2
13. Kawamoto, A., Kodama, E., Sarafianos, S. G., Sakagami, Y., Kohgo, S., Kitano, K., Ashida, N., Iwai, Y., Hayakawa, H., Nakata, H., Mitsuya, H., Arnold, E., and Matsuoka, M. (2008) *Int. J. Biochem. Cell Biol.* **40,** 2410–2420
14. White, K. L., Chen, J. M., Feng, J. Y., Margot, N. A., Ly, J. K., Ray, A. S., Macarthur, H. L., McDermott, M. J., Swaminathan, S., and Miller, M. D. (2006) *Antivir. Ther.* **11,** 155–163
15. Mascolini, M., Larder, B. A., Boucher, C. A., Richman, D. D., and Mellors, J. W. (2008) *Antivir. Ther.* **13,** 1097–1113
16. Le Grice, S. F., and Grüninger-Leitch, F. (1990) *Eur. J. Biochem.* **187,** 307–314
17. Meyer, P. R., Matsuura, S. E., So, A. G., and Scott, W. A. (1998) *Proc. Natl. Acad. Sci. U.S.A.* **95,** 13471–13476
18. Bøyum, A., Løvhaug, D., Tresland, L., and Nordlie, E. M. (1991) *Scand. J. Immunol.* **34,** 697–712
19. Marchand, B., and Götte, M. (2003) *J. Biol. Chem.* **278,** 35362–35372
20. Biaglow, J. E., and Kachur, A. V. (1997) *Radiat. Res.* **148,** 181–187
21. Siddiqui, M. A., Hughes, S. H., Boyer, P. L., Mitsuya, H., Van, Q. N., George, C., Sarafinanos, S. G., and Marquez, V. E. (2004) *J. Med. Chem.* **47,** 5041–5048

22. Stewart, J. J. P. (1989) *J. Comput. Chem.* **10,** 209–220
23. Hattori, S., Ide, K., Nakata, H., Harada, H., Suzu, S., Ashida, N., Kohgo, S., Hayakawa, H., Mitsuya, H., and Okada, S. (2009) *Antimicrob. Agents Chemother.* **53,** 3887–3893
24. Quan, Y., Liang, C., Inouye, P., and Wainberg, M. A. (1998) *Nucleic Acids Res.* **26,** 5692–5698
25. Tong, W., Lu, C. D., Sharma, S. K., Matsuura, S., So, A. G., and Scott, W. A. (1997) *Biochemistry* **36,** 5749–5757
26. Sluis-Cremer, N., Arion, D., and Parniak, M. A. (2000) *Cell. Mol. Life Sci.* **57,** 1408–1422
27. Arion, D., Kaushik, N., McCormick, S., Borkow, G., and Parniak, M. A. (1998) *Biochemistry* **37,** 15908–15917
28. Meyer, P. R., Matsuura, S. E., Mian, A. M., So, A. G., and Scott, W. A. (1999) *Mol. Cell* **4,** 35–43
29. Sarafianos, S. G., Clark, A. D., Jr., Das, K., Tuske, S., Birktoft, J. J., Ilankumaran, P., Ramesha, A. R., Sayer, J. M., Jerina, D. M., Boyer, P. L., Hughes, S. H., and Arnold, E. (2002) *EMBO J.* **21,** 6614–6624
30. Sarafianos, S. G., Clark, A. D., Jr., Tuske, S., Squire, C. J., Das, K., Sheng, D., Ilankumaran, P., Ramesha, A. R., Kroth, H., Sayer, J. M., Jerina, D. M., Boyer, P. L., Hughes, S. H., and Arnold, E. (2003) *J. Biol. Chem.* **278,** 16280–16288
31. Tuske, S., Sarafianos, S. G., Clark, A. D., Jr., Ding, J., Naeger, L. K., White, K. L., Miller, M. D., Gibbs, C. S., Boyer, P. L., Clark, P., Wang, G., Gaffney, B. L., Jones, R. A., Jerina, D. M., Hughes, S. H., and Arnold, E. (2004) *Nat. Struct. Mol. Biol.* **11,** 469–474
32. Yang, G., Wang, J., Cheng, Y., Dutschman, G. E., Tanaka, H., Baba, M., and Cheng, Y. C. (2008) *Antimicrob. Agents Chemother.* **52,** 2035–2042
33. Sluis-Cremer, N., Arion, D., Parikh, U., Koontz, D., Schinazi, R. F., Mellors, J. W., and Parniak, M. A. (2005) *J. Biol. Chem.* **280,** 29047–29052
34. Marchand, B., White, K. L., Ly, J. K., Margot, N. A., Wang, R., McDermott, M., Miller, M. D., and Götte, M. (2007) *Antimicrob. Agents Chemother.* **51,** 2911–2919
35. Feng, J. Y., Murakami, E., Zorca, S. M., Johnson, A. A., Johnson, K. A., Schinazi, R. F., Furman, P. A., and Anderson, K. S. (2004) *Antimicrob. Agents Chemother.* **48,** 1300–1306
36. Nakata, H., Amano, M., Koh, Y., Kodama, E., Yang, G., Bailey, C. M., Kohgo, S., Hayakawa, H., Matsuoka, M., Anderson, K. S., Cheng, Y. C., and Mitsuya, H. (2007) *Antimicrob. Agents Chemother.* **51,** 2701–2708
37. Strerath, M., Cramer, J., Restle, T., and Marx, A. (2002) *J. Am. Chem. Soc.* **124,** 11230–11231
38. Boyer, P. L., Julias, J. G., Marquez, V. E., and Hughes, S. H. (2005) *J. Mol. Biol.* **345,** 441–450
39. Boyer, P. L., Julias, J. G., Ambrose, Z., Siddiqui, M. A., Marquez, V. E., and Hughes, S. H. (2007) *J. Mol. Biol.* **371,** 873–882
40. Tchesnokov, E. P., Obikhod, A., Schinazi, R. F., and Götte, M. (2008) *J. Biol. Chem.* **283,** 34218–34228
41. Summerer, D., and Marx, A. (2005) *Bioorg. Med. Chem. Lett.* **15,** 869–871
42. Di Pasquale, F., Fischer, D., Grohmann, D., Restle, T., Geyer, A., and Marx, A. (2008) *J. Am. Chem. Soc.* **130,** 10748–10757
43. Maag, H., Rydzewski, R. M., McRoberts, M. J., Crawford-Ruth, D., Verheyden, J. P., and Prisbe, E. J. (1992) *J. Med. Chem.* **35,** 1440–1451
44. Chen, M. S., Suttmann, R. T., Papp, E., Cannon, P. D., McRoberts, M. J., Bach, C., Copeland, W. C., and Wang, T. S. (1993) *Biochemistry* **32,** 6002–6010
45. Chen, M. S., Suttmann, R. T., Wu, J. C., and Prisbe, E. J. (1992) *J. Biol. Chem.* **267,** 257–260
46. Maag, H., Nelson, J. T., Steiner, J. L., and Prisbe, E. J. (1994) *J. Med. Chem.* **37,** 431–438
47. Nitanda, T., Wang, X., Kumamoto, H., Haraguchi, K., Tanaka, H., Cheng, Y. C., and Baba, M. (2005) *Antimicrob. Agents Chemother.* **49,** 3355–3360
48. Tanaka, H., Haraguchi, K., Kumamoto, H., Baba, M., and Cheng, Y. C. (2005) *Antivir. Chem. Chemother.* **16,** 217–221
49. Hsu, C. H., Hu, R., Dutschman, G. E., Yang, G., Krishnan, P., Tanaka, H., Baba, M., and Cheng, Y. C. (2007) *Antimicrob. Agents Chemother.* **51,** 1687–1693
50. Yang, G., Dutschman, G. E., Wang, C. J., Tanaka, H., Baba, M., Anderson, K. S., and Cheng, Y. C. (2007) *Antiviral Res.* **73,** 185–191

Synthesis and biological evaluation of selective CXCR4 antagonists containing alkene dipeptide isosteres†

Tetsuo Narumi,[a,b] Ryoko Hayashi,[a] Kenji Tomita,[a] Kazuya Kobayashi,[a] Noriko Tanahara,[a] Hiroaki Ohno,[a] Takeshi Naito,[a] Eiichi Kodama,[c] Masao Matsuoka,[c] Shinya Oishi*[a] and Nobutaka Fujii*[a]

Received 21st August 2009, Accepted 31st October 2009
First published as an Advance Article on the web 4th December 2009
DOI: 10.1039/b917236j

A set of cyclic peptide analogues of a selective CXCR4 antagonist FC131 [*cyclo*(-D-Tyr-Arg-Arg-Nal-Gly-)] were synthesized and bioevaluated. Using (*E*)-alkene and (*Z*)-fluoroalkene dipeptide isosteres for Arg-Arg and Arg-Nal substructures, indispensable or the partial contribution of the two peptide bonds to the CXCR4 antagonism and anti-HIV activity was demonstrated. FC131 and the analogues were shown to selectively inhibit SDF-1 binding to CXCR4, whereas no inhibition of binding of SDF-1 to CXCR7 was observed.

Introduction

Chemokine receptor CXCR4 belongs to the G-protein coupled receptor family[1] and plays important roles in physiological functions including angiogenesis,[2] chemotaxis,[3] and neurogenesis.[4] CXCR4 is associated with various pathological conditions including cancer metastasis,[5] HIV-1 infection[6] and rheumatoid arthritis.[7] The broad spectrum of biological activities has led to extensive research towards the development of specific inhibitors directed against CXCR4.[8,9]

We have previously identified a highly potent CXCR4 antagonist, T140 **1**, which is a β-sheet-like 14-mer peptide with a single disulfide bridge (Fig. 1).[10] The indispensable residues for bioactivity are four amino acids positioned across the disulfide bridge: Arg2, L-3-(2-naphthyl)alanine3 (Nal3), Tyr5 and Arg14. These residues were used for further molecular-size reductions. Using these critical residues for a characteristic combination of cyclic pentapeptide libraries, a potent CXCR4 antagonist FC131 **2** was identified, which exerts comparable anti-HIV activity to T140.[11]

Structure–activity relationship (SAR) studies of FC131 by various modifications such as amino acid substitution,[12] tuning of the ring structure,[13] and backbone modifications,[14,15] demonstrated that the potent bioactivity of FC131 is attributed to the ideal spatial dispositions of the side-chain functional groups. For example, *N*-methylation of the peptide bonds of FC131 and the epimeric congeners significantly altered the bioactivity.[14] The appropriate combination of sequence, chirality and auxiliary groups on the cyclic pentapeptide backbone can accommodate the bioactive conformations.

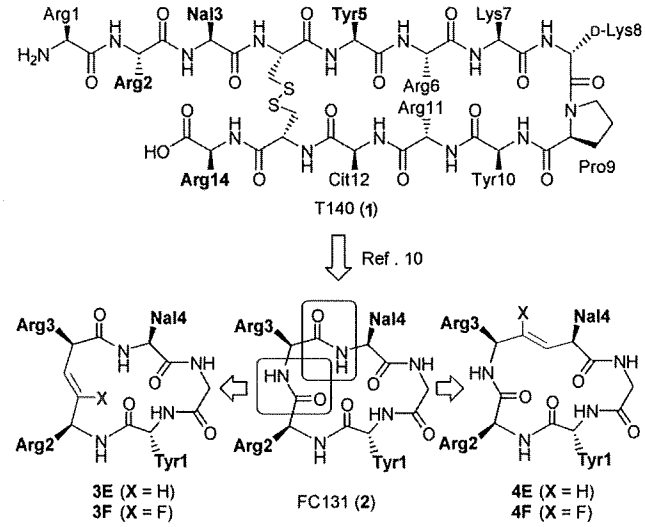

Fig. 1 Structures of T140 (**1**), FC131 (**2**), and the (*E*)-alkene and (*Z*)-fluoroalkene FC131 analogues. Bold residues of **1** are indispensable for the potent CXCR4-antagonistic activity. Nal = L-3-(2-naphthyl)alanine.

Replacement of the planar amide bond with a surrogate alkene substructure, including unsubstituted,[15,16] fluorinated,[17] multi-substituted,[18] and trifluoromethylated[19] alkenes, represents a promising approach to probe structural and electrostatic requirements in bioactive peptides. In particular, fluorinated or substituted alkene isosteres are considered to be more appropriate peptide bond mimetics when compared with unsubstituted alkene isosteres because of the favorable electrostatic and steric properties.[20] In this study, the contributions of the Arg2-Arg3 and Arg3-Nal4 peptide bonds to the bioactivity of FC131 were investigated through the synthesis and bioevaluation of alkene analogues of FC131, *cyclo*[(-D-Tyr-Arg-ψ[*trans*-CX=CH]-Arg-Nal-Gly-)] **3E/3F** and *cyclo*[(-D-Tyr-Arg-Arg-ψ[(*trans*-CX=CH]-Nal-Gly-)] **4E/4F** (X = H or F). The comparative study using unsubstituted and fluorinated isosteres aimed to reveal the electrostatic contributions of the amide carbonyl groups of these peptide bonds to the bioactivity of FC131.

[a]*Graduate School of Pharmaceutical Sciences, Kyoto University, Sakyo-ku, Kyoto 606-8501, Japan. E-mail: soishi@pharm.kyoto-u.ac.jp, nfujii@pharm.kyoto-u.ac.jp; Fax: +81-75-753-4570; Tel: +81-75-753-4551*
[b]*Institute of Biomaterials and Bioengineering, Tokyo Medical and Dental University, Chiyoda-ku, Tokyo 101-0062, Japan*
[c]*Laboratory of Virus Control, Institute for Virus Research, Kyoto University, Sakyo-ku, Kyoto 606-8507, Japan*
† Electronic supplementary information (ESI) available: Additional experimental procedures, NMR spectra and HPLC charts. See DOI: 10.1039/b917236j

Results and discussion

Synthesis of alkene dipeptide isosteres and the application to FC131 analogues

In our previous synthesis of the Arg-Nal type (*E*)-alkene dipeptide isostere (EADI),[15] a protected arginine was employed as the starting material. However, the derivatives were not experimentally tractable in the same synthetic process due to the presence of the protected guanidino group. Consequently, the synthesis of FC131 analogue **3E** bearing Arg-Arg type EADI began with Boc-Orn(Cbz)-OMe **5** (Orn = L-ornithine, Scheme 1). Ornithine includes a 3-aminoprop-1-yl group that can be used as a precursor of the arginine side-chain. Successive treatment of the ester **5** with diisobutylaluminium hydride (DIBAL-H) and vinylzinc chloride, gave a *syn* and *anti*-mixture of allylic alcohols **6** (*syn*:*anti* = 87:13). The *syn*-isomer **6a** was obtained by recrystallization. Boc cleavage of **6a** with TFA followed by *N*-2-nitrobenzenesulfonyl (Ns) protection produced a Ns-amide **7**. The intramolecular Mitsunobu reaction of **7** proceeded to provide 2,3-*cis*-aziridine **8** in high yield. Ozonolysis of **8** and the subsequent Horner–Wadsworth–Emmons reaction predominantly afforded the (*E*)-isomer of β-aziridinyl-α,β-enoate **9** in 57% yield. Organocopper-mediated *anti*-S_N2' type alkylation of **9** gave the α-alkylated product **10** with a TBS-protected 3-hydroxyprop-1-yl group, that can be modified to provide another Arg side-chain. Transformation to the Orn side-chain was performed by TBAF-mediated deprotection

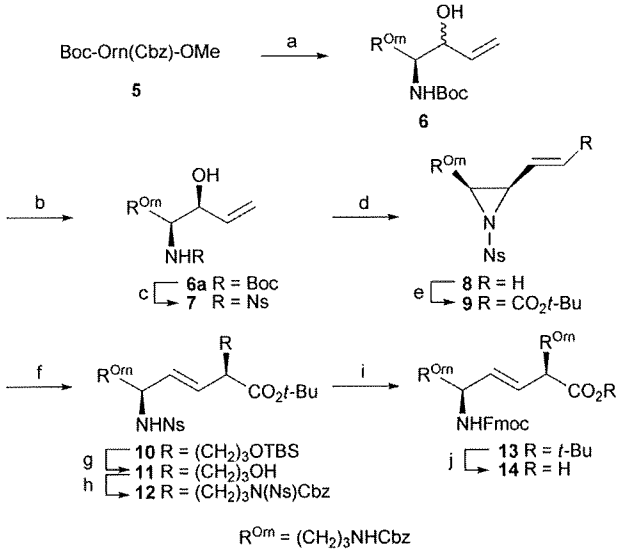

Scheme 1 Synthesis of the Orn-Orn-type (*E*)-alkene dipeptide isostere. Reagents and conditions: (a) (i) Diisobutylaluminium hydride (DIBAL-H), CH_2Cl_2–toluene, −78 °C, 1 h; (ii) H_2C=$CHMgCl$, $ZnCl_2$, LiCl, −78 °C, 3 h (42%, *syn*:*anti* = 87:13); (b) recrystallization; (c) (i) TFA, CH_2Cl_2, 0 °C, 1 h; (ii) 2-nitrobenzenesulfonyl chloride (NsCl), Et_3N, CH_2Cl_2, rt, 1 h (74%); (d) diethyl azodicarboxylate (DEAD), PPh_3, THF, rt, 9 h (93%); (e) (i) O_3, EtOAc, −78 °C, then Me_2S; (ii) $(EtO)_2P(O)CH_2CO_2t$-Bu, LiCl, (*i*-Pr)$_2$NEt, MeCN, 0 °C, 4 h (57%); (f) $TBSO(CH_2)_3Li$, CuCN, LiCl, THF–Et_2O–*n*-pentane, −78 °C, 2 h (66%); (g) tetrabutylammonium fluoride (TBAF), THF, 0 °C, 14 h (85%); (h) CbzNHNs, DEAD, PPh_3, THF, 0 °C, 24 h (93%); (i) (i) PhSH, K_2CO_3, MeCN–DMSO, 50 °C, 2 h; (ii) *N*-(9-fluorenylmethoxycarbonyloxy)succinimide (Fmoc-OSu), Et_3N, THF–H_2O, 0 °C, 4 h (quant); (j) 4 N HCl–dioxane, rt, 8 h (65%).

of **10** and the subsequent Mitsunobu reaction using CbzNHNs to give a bis(sulfonamide) **12**. The expected Fmoc-Orn(Cbz)-ψ[(*E*)-CH=CH]-Orn(Cbz)-OH **14** was obtained by sequential manipulation of the protecting groups including cleavage of two Ns groups in **12** and *N*-Fmoc protection and deprotection of the *t*-Bu ester.

Diastereoselective synthesis of (*Z*)-fluoroalkene dipeptide isosteres (FADI) has recently been accomplished.[17e] The key step in this synthesis is the one-pot reaction involving organocopper-mediated reduction/asymmetric alkylation *via* transmetalation to establish the α-alkylated isostere with appropriate configuration. According to the previous synthetic study of peptide **3F** bearing the Arg-Arg type FADI,[17i] the preparation of the Orn-Nal type FADI was carried out (Scheme 2). The one-pot reaction of γ,γ-difluoro-α,β-enoyl sultam **15**[17i] with 2-(bromomethyl)naphthalene yielded the corresponding α-alkylated sultam **16**. Cleavage of the TBS group with aqueous H_2SiF_6 followed by the Mitsunobu reaction with BocNHNs afforded the sulfonamide **17**. The sulfonamide **17** was converted to the Fmoc-protected FADI **18** by a standard deprotection/protection manipulation.

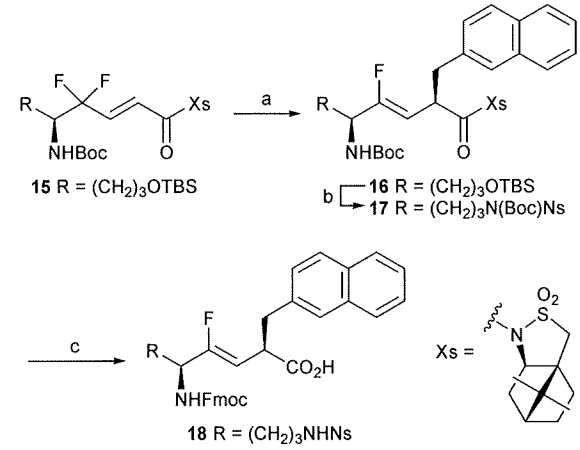

Scheme 2 Synthesis of the Orn-Nal-type (*Z*)-fluoroalkene dipeptide isostere. Reagents and conditions: (a) (i) Me_2CuLi·LiI·2LiBr, THF–Et_2O, −78 °C, 0.5 h; (ii) Hexamethylphosphoric triamide (HMPA), −78 °C, 0.5 h; (iii) Ph_3SnCl, THF, −40 °C, 10 min; (iv) 2-(bromomethyl)naphthalene, −40 °C, 20 h (79%); (b) (i) H_2SiF_6 aq. MeCN–MeOH, 0 °C, 1 h; (ii) BocNHNs, DEAD, PPh_3, THF, rt, 12 h (98%); (c) (i) 1 N LiOH, H_2O_2, THF–H_2O, rt, 2 h; (ii) TFA, CH_2Cl_2, rt, 0.5 h; (iii) Fmoc-OSu, Et_3N, DMF–H_2O–MeCN, rt, 12 h (85%).

The resulting isosteres **14** and **18** were incorporated into the peptide-chain by standard Fmoc-based solid-phase peptide synthesis (Scheme 3). Briefly, the protected peptides **21a,b** were cleaved off the resins **20a,b** with 1,1,1,3,3,3-hexafluoroisopropanol (HFIP). After diphenylphosphoryl azide (DPPA)-mediated cyclization, the Cbz- or Ns-groups on the ornithine δ-amino group(s) of **22a,b** were deprotected by treatment with 1 M TMSBr/thioanisole in TFA or with 95% aqueous TFA followed by 2-mercaptoethanol/1,8-diazabicyclo[5,4,0]-7-undecene (DBU), respectively. Subsequently, the amino group(s) of **23a,b** were modified using 1*H*-pyrazole-1-carboxamidine to provide the expected peptidomimetics **3E** and **4F** with the Arg guanidino group(s).